IFSCOM-E 2024
10TH IFS AND CONTEMPORARY MATHEMATICS AND ENGINEERING CONFERENCE
04-07 SEPTEMBER 2024, MERSİN, TÜRKİYE
ISBN: 978-625-97923-1-6
pp: 62-69

A MULTI-CRITERIA DECISION MAKING APPROACH USING A NEW SIMILARITY MEASURE UNDER THE NEUTROSOPHIC Z-NUMBER UNIVERSE

GÜLER TUĞBA GÜLTEKİN, ELIF BAŞKAN, RIDVAN ŞAHİN
0009-0000-0043-0308, 0000-0003-0767-6882 and 0000-0001-7434-4269

ABSTRACT

The neutrosophic sets developed by Smarandache define the membership of an element in a set with three components: truth, indeterminacy, and falsity. These membership functions take values in the range [0,1], and their sum can exceed 3. Neutrosophic sets generalize classical and fuzzy sets, allowing for a more flexible modeling of indeterminacy and contradiction. The Z-numbers proposed by Zadeh better express both the information of the data and the reliability of that information. However, they have limitations regarding reliability in environments with indeterminacy and inconsistency. The neutrosophic Z-numbers (NZNs) proposed by Ye and colleagues address this limitation by considering not only the degrees of truth, indeterminacy, and falsity but also the reliability degree of each separately. This allows NZN to better model uncertainties in decision-making processes, leading to more reliable outcomes. Although these numbers are an important tool in decision-making processes, the methods developed to measure the similarity between different NZNs in the current literature are limited.

In this study, a new similarity measure is proposed on the NZN set. Then, considering the importance of each element, the similarity measure is extended to a weighted similarity measure. Subsequently, a multi-criteria decision-making method using the proposed similarity measure is developed within the framework of NZN sets. The effectiveness of the proposed method is demonstrated through an example application. It was concluded that for many real-world problems where decision-makers face different and conflicting criteria, the proposed method leads to more consistent and reliable decisions.

1. INTRODUCTION

Multiple researchers in diverse fields have applied multi-criteria decision making methods (MCDMs). However, decision makers find it difficult to portray situations using uncertain and insufficient information. Zadeh [1] brought in fuzzy sets (FSs) to deal with uncertain information and tackle this problem. A fuzzy set is characterized by its membership information and is frequently used in decision-making situations, pattern recognition, and approximate reasoning. However, there are situations in which fuzzy sets may not be enough in expressing particular conditions as they lack indeterminacy information. Considering this, Atanassov [2] put forth the concept of intuitionistic fuzzy sets (IFS).

Intuitionistic fuzzy sets are composed of information on both membership and non-membership, with the combined total not exceeding one. This design has been utilized in a range of areas such as decision-making activities [3], medical diagnoses [4], and neural networks [5, 6].

Date: September, 20, 2024.
Key words and phrases. Neutrosophic Z-numbers, Similarity measure, Decision making

Intuitionistic fuzzy sets have membership and non-membership degrees for each element that must total within the range of [0, 1], causing challenges in modeling scenarios with uncertainty. For instance, if a specialist assesses a situation, they may determine the truth membership as 0.7, the indeterminacy membership as 0.2, and the falsity membership as 0.6. This scenario cannot be clarified using fuzzy and intuitionistic fuzzy sets [7]. Smarandache [8] introduced the idea of neutrosophic sets (NSs) to address this situation. Neutrosophic sets assign values for truth, falsity, and hesitation, offering a logic that enables highly objective assessments. Neutrosophic sets are defined by membership degrees of truth, indeterminacy, and falsity, with the total of these degrees not exceeding three. Neutrosophic sets can have values in the range of $]0^-, 1^+[$. Therefore it has a philosophical meaning, and many special cases have been developed to use it in practical applications [7].

Zadeh [9] introduced the idea of Z-numbers to represent the limitation and dependability of assessing fuzzy numbers using an ordered pair in determinacy situations. A Z-number consists of an ordered pair of fuzzy numbers (X, Y)depending on an indeterminacy variable N, with X representing a value of N and Y as a measure of reliability for X. The Z-number is a broader concept linked to reliability compared to the classical fuzzy number. Z-numbers can be more effectively describe the uncertainties related to reliability and as a result, have garnered significant interest [10-13].

Neutrosophic sets are distinguished by their levels of truth, falsity, and indeterminacy in uncertain and inconsistent surroundings, while Z-numbers are unable to capture this attribute. While neutrosophic sets have been utilized in different fields, there is a deficiency in reliability measures concerning truth, indeterminacy, and falsity membership degrees. Du et al. [12] expanded the Z-number concept to neutrosophic sets and introduced hybrid knowledge, consisting of truth, falsity, and indeterminacy degrees along with their respective reliability degrees, represented by three sets of fuzzy numbers. Having this in consideration, they present an expanded neutrosophic notion that is strongly connected to reliability and utilize it in MCDM issues.

In 2021, Du et al. introduced the idea of neutrosophic Z-number (NZN) set, which extends the concept of Z-number and neutrosophic set. NZN integrates neutrosophic values with neutrosophic reliability measures in a novel framework. Next, the neutrosophic Z-numbers operations and a ranking score function for NZNs are introduced, along with the NZN weighted arithmetic average (NZNWAA) and NZN weighted geometric average (NZNWGA) operators for combining NZN data. Furthermore, Du et al. [12] created an MCDM method in NZN setting utilizing NZNWAA and NZNWGA operators along with a score function. A sample is utilized to showcase how the developed MCDM approach can be effectively used in the NZN environment.

There are certain information measures that have not yet been defined in NZN sets. Hence, in this research, we establish a new similarity measure. The framework of our work in this context is laid out as follows: Section 2 provides the definitions of the NZN set and the operational relationships of NZNs. Section 3 introduces the novel exponential similarity measure (ESM) created for NZN sets, and then discusses a weighted ESM for NZN sets. In Section 4, a method is introduced for evaluating and diagnosing symptoms of Benign Prostatic Hyperplasia (BPH) using ESM in a neutrosophic Z-number environment. The method is then demonstrated on an example of BPH symptom evaluation to showcase its effectiveness and rationality. Summary of findings and recommendations will be presented in Section 5.

2. BASIC CONCEPTS OF NEUTROSOPHIC Z-NUMBER SETS

The Z-number, proposed by Zadeh [9] is a type of uncertain variable N that is based on the fuzzy numbers depending on the fuzzy numbers (X, Y) and is defined as a pair of values in specific order. If X's reliability measure is fuzzy, then it is a value of Y. This definition does not include information about the uncertainty and inaccuracy of Z-numbers. An NZN set is created as an expansion of the Z-number to represent the combined information of truth, indeterminacy, and falsity in Z-numbers [12].

Definition 2.1. [12] Let N be a universe set, a NZN set in N is defined as follows:

$$S_Z = \{\langle n, T(X,Y)(n), I(X,Y)(n), F(X,Y)(n)\rangle | n \in N\},$$

Here $T(X,Y)(n) = \big(T_X(n), T_Y(n)\big), I(X,Y)(n) = \big(I_X(n), I_Y(n)\big), F(X,Y)(n) = \big(F_X(n), F_Y(n)\big) : N \longrightarrow [0,1]^2$ are ordered pairs of fuzzy values of truth, indeterminacy and falsity, then the first component X are fuzzy values in a universe set N and the second component $Y$are the measures of reliability for X, with the conditions $0 \leq T_X(n) + I_X(n) + F_X(n) \leq 3$ and $0 \leq T_Y(n) + I_Y(n) + F_Y(n) \leq 3$ together.

For proper screening, S_Z in $\langle n, T(X,Y)(n), I(X,Y)(n), F(X,Y)(n)\rangle$ element is simply $S_Z = \langle T(X,Y),\ I(X,Y),\ F(X,Y)\rangle = \langle (T_X, T_Y),\ (I_X, I_Y),\ (F_X, F_Y)\rangle$ and is called the NZN set.

Definition 2.2. [12] For two NZN sets $S_{z_1} = \langle T_1(X,Y),\ I_1(X,Y),\ F_1(X,Y)\rangle = \langle \big(T_{X_1}, T_{Y_1}\big),\ \big(I_{X_1}, I_{Y_1}\big),\ \big(F_{X_1}, F_{Y_1}\big)\rangle$ and $S_{z_2} = \langle T_2(X,Y),\ I_2(X,Y),\ F_2(X,Y)\rangle = \langle \big(T_{X_2}, T_{Y_2}\big),\ \big(I_{X_2}, I_{Y_2}\big),\ \big(F_{X_2}, F_{Y_2}\big)\rangle$, $\lambda > 0$, there are the following relationships:

1. $S_{z_1} \supseteq S_{z_2} \Leftrightarrow T_{V_1} \geq T_{V_2}, T_{R_1} \geq T_{R_2}, I_{V_1} \leq I_{V_2}, I_{R_1} \leq I_{R_2}, F_{V_1} \leq F_{V_2}, F_{R_1} \leq F_{R_2}$;
2. $S_{z_1} = S_{z_2} \Leftrightarrow S_{z_1} \supseteq S_{z_2}\ ve\ S_{z_2} \supseteq S_{z_1}$;
3. $S_{z_1} \cup S_{z_2} = \langle \big(T_{V_1} \vee T_{V_2}, T_{R_1} \vee T_{R_2}\big),\ \big(I_{V_1} \wedge I_{V_2}, I_{R_1} \wedge I_{R_2}\big),\ \big(F_{V_1} \wedge F_{V_2}, F_{R_1} \wedge F_{R_2}\big)\rangle$;
4. $S_{z_1} \cap S_{z_2} = \langle \big(T_{V_1} \wedge T_{V_2}, T_{R_1} \wedge T_{R_2}\big),\ \big(I_{V_1} \vee I_{V_2}, I_{R_1} \vee I_{R_2}\big),\ \big(F_{V_1} \vee F_{V_2}, F_{R_1} \vee F_{R_2}\big)\rangle$;
5. $\big(S_{z_1}\big)^C = \langle \big(F_{V_1}, F_{R_1}\big), \big(1 - I_{V_1}, 1 - I_{R_1}\big), \big(T_{V_1}, T_{R_1}\big)\rangle$;
6. $S_{z_1} \oplus S_{z_2} = \langle \big(T_{V_1} + T_{V_2} - T_{V_1}T_{V_2}, T_{R_1} + T_{R_2} - T_{R_1}T_{R_2}\big),\ \big(I_{V_1}I_{V_2}, I_{R_1}I_{R_2}\big),\ \big(F_{V_1}F_{V_2}, F_{R_1}F_{R_2}\big)\rangle$;
7. $S_{z_1} \otimes S_{z_2} = \langle \big(T_{V_1}T_{V_2}, T_{R_1}T_{R_2}\big),\ \big(I_{V_1} + I_{V_2} - I_{V_1}I_{V_2}, I_{R_1} + I_{R_2} - I_{R_1}I_{R_2}\big),\ \big(F_{V_1} + F_{V_2} - F_{V_1}F_{V_2}, F_{R_1} + F_{R_2} - F_{R_1}F_{R_2}\big)\rangle$;
8. $\lambda S_{z_1} = \langle (1 - (1 - T_{V_1})^{\lambda}, (1 - (1 - T_{R_1})^{\lambda},\ (I_{V_1}^{\lambda}, I_{R_1}^{\lambda}), (F_{V_1}^{\lambda}, F_{R_1}^{\lambda})\ \rangle$;
9. $S_{z_1}^{\lambda} = \langle \big(T_{V_1}^{\lambda}, T_{R_1}^{\lambda}\big), \Big(1 - \big(1 - I_{V_1}\big)^{\lambda}, 1 - \big(1 - I_{R_1}\big)^{\lambda}\Big), \Big(1 - \big(1 - F_{V_1}\big)^{\lambda}, 1 - \big(1 - F_{R_1}\big)^{\lambda}\Big)\rangle$.

3. EXPONENTIAL SIMILARITY MEASURES OF NZN SETS

Based on an exponential function, this chapter proposes ESMs for NZN sets and investigates their properties.

Definition 3.1. Let $S_{z_1} = \big\{\langle n_i, \big(T_{X_1}, T_{Y_1}\big)(n_i),\ \big(I_{X_1}, I_{Y_1}\big)(n_i),\ \big(F_{X_1}, F_{Y_1}\big)(n_i)\rangle | n_i \in N\big\}$ and $S_{z_2} = \big\{\langle n_i, \big(T_{X_2}, T_{Y_2}\big)(n_i),\ \big(I_{X_2}, I_{Y_2}\big)(n_i),\ \big(F_{X_2}, F_{Y_2}\big)(n_i)\rangle | n_i \in N\big\}$ be two NZN sets in $N = \{n_1, n_2, n_3, \dots, n_k\}$. In this case, the ESM between $S_{z_1}$and S_{z_2} can be defined as follows:

$$E(S_{Z_1}, S_{Z_2}) = \frac{1}{k}\left[\sum_{i=1}^{k} \frac{\exp\left(-\frac{1}{3}\left(\left|T_{X_1}(n_i)T_{Y_1}(n_i) - T_{X_2}(n_i)T_{Y_2}(n_i)\right| + \left|I_{X_1}(n_i)I_{Y_1}(n_i) - I_{X_2}(n_i)I_{Y_2}(n_i)\right| + \left|F_{X_1}(n_i)F_{Y_1}(n_i) - F_{X_2}(n_i)F_{Y_2}(n_i)\right|\right)\right) - \exp(-1)}{1 - \exp(-1)}\right]. \quad (1)$$

Proposition 3.1. Let $S_{z_1} = \{\langle n_i, (T_{X_1}, T_{Y_1})(n_i),\ (I_{X_1}, I_{Y_1})(n_i),\ (F_{X_1}, F_{Y_1})(n_i)\rangle | n_i \in N\}$ and $S_{z_2} = \{\langle n_i, (T_{X_2}, T_{Y_2})(n_i),\ (I_{X_2}, I_{Y_2})(n_i),\ (F_{X_2}, F_{Y_2})(n_i)\rangle | n_i \in N\}$ be two NZN sets in $N = \{n_1, n_2, n_3, \dots, n_k\}$. The ESM $E(S_{z_1}, S_{z_2})$ must satisfy the following properties:

(1) $0 \le E(S_{z_1}, S_{z_2}) \le 1$;
(2) $E(S_{z_1}, S_{z_2}) = 1$ if $S_{z_1} = S_{z_2}$;
(3) $E(S_{z_1}, S_{z_2}) = E(S_{z_2}, S_{z_1})$;
(4) If $S_{z_3}$is a NZN set in N, and $S_{z_1} \subseteq S_{z_2} \subseteq S_{z_3}$, then $E(S_{z_1}, S_{z_3}) \le E(S_{z_1}, S_{z_2})$ and $E(S_{z_1}, S_{z_3}) \le E(S_{z_2}, S_{z_3})$.

Proof.
(1) Since S_{z_1} and S_{z_2} are two NZN sets, $T_{X_1}(n_i),\ I_{X_1}(n_i),\ F_{X_1}(n_i) \in [0,1]$, $T_{X_2}(n_i),\ I_{X_2}(n_i),\ F_{X_2}(n_i) \in [0,1]$, $T_{Y_1}(n_i), I_{Y_1}(n_i), F_{Y_1}(n_i) \in [0,1]$, $T_{Y_2}(n_i),\ I_{Y_2}(n_i), F_{Y_2}(n_i) \in [0,1]$. Thus, the expression $\left(\left|T_{X_1}(n_i)T_{Y_1}(n_i) - T_{X_2}(n_i)T_{Y_2}(n_i)\right| + \left|I_{X_1}(n_i)I_{Y_1}(n_i) - I_{X_2}(n_i)I_{Y_2}(n_i)\right| + \left|F_{X_1}(n_i)F_{Y_1}(n_i) - F_{X_2}(n_i)F_{Y_2}(n_i)\right|\right)/3$ has a value between 0 and 1. (The maximum value for NZN sets is $S_{Z_{max}} = \langle(1,1),(0,1),(0,1)\rangle$ and the minimum value is $S_{Z_{min}} = \langle(0,1),(1,1),(1,1)\rangle$). Therefore, $0 \le E(S_{z_1}, S_{z_2}) \le 1$ inequality holds.
(2) For two NZN sets S_{z_1} and S_{z_2}, if $S_{z_1} = S_{z_2}$, then $T_{X_1}(n_i) = T_{X_2}(n_i)$, $I_{X_1}(n_i) = I_{X_2}(n_i)$, $F_{X_1}(n_i) = F_{X_2}(n_i)$, $T_{Y_1}(n_i) = T_{Y_2}(n_i)$, $I_{Y_1}(n_i) = I_{Y_2}(n_i)$ and $F_{Y_1}(n_i) = F_{Y_2}(n_i)$ for $n_i \in N$, $i = 1,2,\cdots,k$.
Therefore, $\left|T_{X_1}(n_i)T_{Y_1}(n_i) - T_{X_2}(n_i)T_{Y_2}(n_i)\right| = 0$, $\left|I_{X_1}(n_i)I_{Y_1}(n_i) - I_{X_2}(n_i)I_{Y_2}(n_i)\right| = 0$ and $\left|F_{X_1}(n_i)F_{Y_1}(n_i) - F_{X_2}(n_i)F_{Y_2}(n_i)\right| = 0$ is found. Thus, the following result is obtained:

$$E(S_{z_1}, S_{z_2}) = \frac{1}{k}\left[\sum_{i=1}^{k} \frac{\exp\left(-\frac{1}{3}\left(\left|T_{X_1}(n_i)T_{Y_1}(n_i) - T_{X_2}(n_i)T_{Y_2}(n_i)\right| + \left|I_{X_1}(n_i)I_{Y_1}(n_i) - I_{X_2}(n_i)I_{Y_2}(n_i)\right| + \left|F_{X_1}(n_i)F_{Y_1}(n_i) - F_{X_2}(n_i)F_{Y_2}(n_i)\right|\right)\right) - \exp(-1)}{1 - \exp(-1)}\right]$$
$$= \frac{1}{k}[(k(1 - \exp(-1)/(1 - \exp(-1)))] = 1.$$

(3) Proof is straightforward.
(4)If $S_{z_1} \subseteq S_{z_2} \subseteq S_{z_3}$, then this means $T_{X_1}(n_i) \le T_{X_2}(n_i)) \le T_{X_3}(n_i)$, $I_{X_1}(n_i) \ge I_{X_2}(n_i) \ge I_{X_3}(n_i)$, $F_{X_1}(n_i) \ge F_{X_2}(n_i) \ge F_{X_3}(n_i)$, $T_{Y_1}(n_i) \le T_{Y_2}(n_i)) \le T_{Y_3}(n_i)$, $I_{Y_1}(n_i) \ge I_{Y_2}(n_i) \ge I_{Y_3}(n_i)$ and $F_{Y_1}(n_i) \ge F_{Y_2}(n_i) \ge F_{Y_3}(n_i)$ for $n_i \in N, i = 1,2,\cdots,k$. Hence,

$$\left|T_{X_1}(n_i)T_{Y_1}(n_i) - T_{X_2}(n_i)T_{Y_2}(n_i)\right| \le \left|T_{X_1}(n_i)T_{Y_1}(n_i) - T_{X_3}(n_i)T_{Y_3}(n_i)\right|,$$
$$\left|T_{X_2}(n_i)T_{Y_2}(n_i) - T_{X_3}(n_i)T_{Y_3}(n_i)\right| \le \left|T_{X_1}(n_i)T_{Y_1}(n_i) - T_{X_3}(n_i)T_{Y_3}(n_i)\right|,$$
$$\left|I_{X_1}(n_i)I_{Y_1}(n_i) - I_{X_2}(n_i)I_{Y_2}(n_i)\right| \le \left|I_{X_1}(n_i)I_{Y_1}(n_i) - I_{X_3}(n_i)I_{Y_3}(n_i)\right|,$$
$$\left|I_{X_2}(n_i)I_{Y_2}(n_i) - I_{X_3}(n_i)I_{Y_3}(n_i)\right| \le \left|I_{X_1}(n_i)I_{Y_1}(n_i) - I_{X_3}(n_i)I_{Y_3}(n_i)\right|,$$
$$\left|F_{X_1}(n_i)F_{Y_1}(n_i) - F_{X_2}(n_i)F_{Y_2}(n_i)\right| \le \left|F_{X_1}(n_i)F_{Y_1}(n_i) - F_{X_3}(n_i)F_{Y_3}(n_i)\right|,$$
$$\left|F_{X_2}(n_i)F_{Y_2}(n_i) - F_{X_3}(n_i)F_{Y_3}(n_i)\right| \le \left|F_{X_1}(n_i)F_{Y_1}(n_i) - F_{X_3}(n_i)F_{Y_3}(n_i)\right|.$$

In this case $E(S_{z_1}, S_{z_3}) \le E(S_{z_1}, S_{z_2})$ and $E(S_{z_1}, S_{z_3}) \le E(S_{z_2}, S_{z_3})$ because $\exp\left(-\frac{1}{3}\left(\left|T_{X_1}(n_i)T_{Y_1}(n_i) - T_{X_2}(n_i)T_{Y_2}(n_i)\right| + \left|I_{X_1}(n_i)I_{Y_1}(n_i) - I_{X_2}(n_i)I_{Y_2}(n_i)\right| + \left|F_{X_1}(n_i)F_{Y_1}(n_i) - F_{X_2}(n_i)F_{Y_2}(n_i)\right|\right)\right)$ is a decreasing function.

Therefore, the proofs of these properties are completed.

Definition 3.2. Let $S_{z_1} = \{\langle n_i, (T_{X_1}, T_{Y_1})(n_i),\ (I_{X_1}, I_{Y_1})(n_i),\ (F_{X_1}, F_{Y_1})(n_i)\rangle | n_i \in N\}$ and $S_{z_2} = \{\langle n_i, (T_{X_2}, T_{Y_2})(n_i),\ (I_{X_2}, I_{Y_2})(n_i),\ (F_{X_2}, F_{Y_2})(n_i)\rangle | n_i \in N\}$ be two NZN sets in $N = \{n_1,\ n_2, n_3, \dots, n_k\}$. Usually $\forall n_i \in N$, the weight of each element is taken into account and for the weight of an element n_i is assumed to be w_i $(i = 1,2, \dots, k)$, where $w_i \in [0,1]$ and $\sum_{i=1}^{k} w_i = 1$. In this case, the weighted ESM between S_{z_1} and S_{z_2} can be defined as follows:

$$E_w(S_{z_1}, S_{z_2}) = \frac{1}{k}\left[\sum_{i=1}^{k} w_i \frac{\exp\left(-\frac{1}{3}\left(\left|T_{X_1}(n_i)T_{Y_1}(n_i) - T_{X_2}(n_i)T_{Y_2}(n_i)\right| + \left|I_{X_1}(n_i)I_{Y_1}(n_i) - I_{X_2}(n_i)I_{Y_2}(n_i)\right| + \left|F_{X_1}(n_i)F_{Y_1}(n_i) - F_{X_2}(n_i)F_{Y_2}(n_i)\right|\right)\right) - \exp(-1)}{1 - \exp(-1)}\right]. \quad (2)$$

Proposition 3.2. $S_{z_1} = \langle (T_{X_1}, T_{Y_1}),\ (I_{X_1}, I_{Y_1}),\ (F_{X_1}, F_{Y_1})\rangle$ and $S_{z_2} = \langle (T_{X_2}, T_{Y_2}),\ (I_{X_2}, I_{Y_2}),\ (F_{X_2}, F_{Y_2})\rangle$ denotes two NZN sets. Here $N = \{n_1,\ n_2, n_3, \dots, n_k\}$ and their weights is given by the vector $w_i = \{w_1, w_2, \dots, w_k\}$, where $\sum_{i=1}^{k} w_i = 1$. The weighted ESM of NZN sets $E_w(S_{z_1}, S_{z_2})$ provides the following features.

(M1) $0 \leq E_w(S_{z_1}, S_{z_2}) \leq 1$;
(M2) $E_w(S_{z_1}, S_{z_2}) = 1$ if $S_{z_1} = S_{z_2}$;
(M3) $E_w(S_{z_1}, S_{z_2}) = E_w(S_{z_2}, S_{z_1})$;
(M4) If $S_{z_3}$is a NZN set in N, and $S_{z_1} \subseteq S_{z_2} \subseteq S_{z_3}$, then $E_w(S_{z_1}, S_{z_3}) \leq E_w(S_{z_1}, S_{z_2})$ and $E_w(S_{z_1}, S_{z_3}) \leq E_w(S_{z_2}, S_{z_3})$.

Proof. The proof is clear from the previous proof.

To illustrate the proposed method, we will use the following example adapted from the study [14].

4. PRELIMINARY ASSESSMENT/DIAGNOSIS APPROACH FOR BPH USING ESM WITH NZN SET

Based on the seven questions in the AUA symptom indexes for BPH, a physician can assess patients' BPH symptoms using Q = {Q_1 (frequency of not emptying bladder completely after urination for the last month), Q_2 (frequency of urinating again within two hours for the last month), Q_3(frequency of starting and stopping urination for the last month), Q_4(difficulty in postponing urinationfor the last month), Q_5(weak urinary stream for the last month) Q_6(pushing or straining to urinate for the last month), Q_7(frequency of getting up at night to urinate for the last month)}. Table 1 presents the clinical assessment of the BPH symptoms for patient Pk (k ranging from 1 to t) at five different instances.

Questions
$\boldsymbol{Q_1}$ (frequency of not emptying bladder completely after urination for the last month)
$\boldsymbol{Q_2}$ (frequency of urinating again within two hours for the last month)
$\boldsymbol{Q_3}$ (frequency of starting and stopping urination for the last month)
$\boldsymbol{Q_4}$ (difficulty in postponing urinationfor the last month)
$\boldsymbol{Q_5}$ (weak urinary stream for the last month)
$\boldsymbol{Q_6}$ (pushing or straining to urinate for the last month)
$\boldsymbol{Q_7}$ (frequency of getting up at night to urinate for the last month)

TABLE 1. The questionnaire of BPH symptoms.

In [14] BPH is categorized into four different types of symptoms, which are denoted by a group of symptoms S = {S_1 (Normal symptom), S_2 (Mild symptom), S_3 (Moderate symptom), S_4 (Severe symptom)} for the initial assessment of BPH patients, as illustrated in Table 2.

	Q_1	Q_2	Q_3	Q_4	Q_5	Q_6	Q_7
S_1	<(0,1),(0,1),(1,1)>	<(0,1),(0,1),(1,1)>	<(0,1),(0,1),(1,1)>	<(0,1),(0,1),(1,1)>	<(0,1),(0,1),(1,1)>	<(0,1),(0,1),(1,1)>	<(0,1),(0,1),(1,1)>
S_2	<(0,1),(0.2,1),(0.8,1)>	<(0,1),(0.2,1),(0.8,1)>	<(0,1),(0.2,1),(0.8,1)>	<(0,1),(0.2,1),(0.8,1)>	<(0,1),(0.2,1),(0.8,1)>	<(0,1),(0.2,1),(0.8,1)>	<(0,1),(0.2,1),(0.8,1)>
S_3	<(0.2,1),(0.4,1),(0.4,1)>	<(0.2,1),(0.4,1),(0.4,1>	<(0.2,1),(0.4,1),(0.4,1>	<(0.2,1),(0.4,1),(0.4,1>	<(0.2,1),(0.4,1),(0.4,1>	<(0.2,1),(0.4,1),(0.4,1>	<(0.2,1),(0.4,1),(0.4,1>
S_4	<(0.6,1),(0.4,1),(0,1)>	<(0.6,1),(0.4,1),(0,1)>	<(0.6,1),(0.4,1),(0,1)>	<(0.6,1),(0.4,1),(0,1)>	<(0.6,1),(0.4,1),(0,1)>	<(0.6,1),(0.4,1),(0,1)>	<(0.6,1),(0.4,1),(0,1)>

TABLE 2. Types of BHP symptoms with NZN information.

We chose to take the Z-numbers for the symptoms in Table 2 as 1 for all cases. This decision was made to simplify the initial analysis and ensure a consistent and controlled assessment environment. By setting the Z-numbers for the symptoms to 1, we effectively assume that the reliability of each truth, indeterminacy, and falsity value for the symptoms is at its maximum. This allows us to focus on the similarity between patient data and the symptoms without the added complexity of varying reliability for the symptoms themselves.

While the reliability of patient data may vary due to different factors, assuming maximum reliability for the symptoms provides a stable reference point for comparison.

Suppose we administer a clinical questionnaire to t patients with BPH using Table 1 to collect their responses regarding BPH symptoms, expressed through truth, indeterminacy, and falsity values with the reliability degree of each values separately. In order to properly assess a patient P_k displaying symptoms of BPH, we can determine the similarity measure $E_w(P_k, S_i)$ for $i = 1, \cdots, 4$ and $k = 1, \cdots, t$. The correct assessment of BPH symptoms for patient P_k is determined as $\text{argmax}_i\{E_w(P_k, S_i)\}$. To demonstrate how the BPH symptoms are evaluated and diagnosed, we present an example of the evaluation and diagnosis process using the proposed method in NZN environment.

Example: In [14], the responses of patients, P_1 P_2, and P_3 to the symptoms are listed in Table 1. The numbers are evaluated as an average of five periodic assessments, are processed using neutrosophic information:

$P_1 = \{\langle Q_1, 0.4, 0.2, 0.4\rangle, \langle Q_2, 0.4, 0.4, 0.2\rangle, \langle Q_3, 0.4, 0.2, 0.4\rangle, \langle Q_4, 0.4, 0.2, 0.4\rangle, \langle Q_5, 0.6, 0.4, 0.0\rangle,$
$\langle Q_6, 0.4, 0.0, 0.6\rangle, \langle Q_7, 0.6, 0.0, 0.4\rangle\},$
$P_2 = \{\langle Q_1, 0.2, 0.2, 0.6\rangle, \langle Q_2, 0.4, 0.2, 0.4\rangle, \langle Q_3, 0.2, 0.0, 0.8\rangle, \langle Q_4, 0.4, 0.2, 0.4\rangle, \langle Q_5, 0.2, 0.4, 0.4\rangle,$

$\langle Q_6, 0.4, 0.0, 0.6 \rangle, \langle Q_7, 0.2, 0.2, 0.6 \rangle \}$,
$P_3 = \{ \langle Q_1, 0.6, 0.0, 0.4 \rangle, \langle Q_2, 0.6, 0.2, 0.2 \rangle, \langle Q_3, 0.6, 0.2, 0.2 \rangle, \langle Q_4, 0.8, 0.2, 0.0 \rangle, \langle Q_5, 0.6, 0.2, 0.2 \rangle,$
$\langle Q_6, 0.8, 0.2, 0.0 \rangle, \langle Q_7, 0.4, 0.4, 0.2 \rangle \}$.

Suppose the weight of every element Q_j equals $w_j = 1/7$ for $j = 1, 2, \cdots, 7$. Using Equation (2) allows us to determine the similarity measure results between the patient P_k $(k = 1, 2, 3)$ and the symptom S_i $(i = 1, 2, 3, 4)$.

If we assume the reliability values for P_k $(k = 1, 2, 3)$ as 1 in Equation (2), we get the similarity values given in Table 3. The results fall within the NS, yielding the same similarity matrix as those in the example [14].

	S_1	S_2	S_3	S_4
P_1	0.4457	0.5460	0.7285	0.6857
P_2	0.5896	0.7038	0.7814	0.5244
P_3	0.3319	0.4406	0.6112	0.7778

TABLE 3. The similarity measurement results for the patients P_k $(k = 1, 2, 3)$, whose symptoms are considered as NZN sets with reliability values of 1.

The highest similarity measure in Table 3 suggests the correct assessment/diagnosis. Hence, during the initial clinical assessments, Patients P_1 and P_2 exhibit moderate symptoms, while Patient P_3 shows severe symptoms.

When we assign the reliability values less than 0.5, patients P_1 P_2, and P_3 are classified as having moderate symptoms. However, if we increase the reliability values to greater than or equal 0.5 for each patient, we notice that P_1 and P_2 continue to exhibit moderate symptoms, while P_3 is classified as having severe symptoms. This demonstrates a consistent and logical outcome with the results in [14].

5. CONCLUSIONS

In this study, we applied our newly developed similarity measure to evaluate the symptoms of Benign Prostatic Hyperplasia (BPH). This innovative approach, utilizing Neutrosophic Z Numbers (NZNs), has enabled a more sensitive similarity analysis. When comparing our results with existing examples from [14], we observed consistency and alignment, which confirms the accuracy and reliability of our new similarity measure. Utilizing Z numbers enables a more accurate management of uncertainty and variability, resulting in a more defined categorization and evaluation of patient symptoms.

Moreover, we obtain a strong and simple analysis by first assuming the symptoms have maximum reliability. Nevertheless, future research may encounter variability in the reliability of symptoms due to factors like varying clinical interpretations or patient reporting. Therefore, it would be beneficial to investigate how varying symptom reliability impacts the assessment and diagnosis process.

REFERENCES

[1] L.A. Zadeh, Fuzzy sets, Information and control, 8(3), 338-353, (1965).

[2] K. T. Atanassov, Intuitionistic fuzzy sets. Fuzzy Sets Syst 20(1):87–96, (1986).

[3] H. W. Liu, G. J. Wang, Multi-criteria decision-making methods based on intuitionistic fuzzy sets, European Journal of Operational Research, 179(1), 220-233, (2007).

[4] T. K. Shinoj, S. J. John, Intuitionistic fuzzy multisets and its application in medical diagnosis, World Academy of Science, Engineering and Technology, 6(1), 1418-1421, (2012).

[5] S. Sotirov, E. Sotirova, D. Orozova, Neural network for defining intuitionistic fuzzy sets in e-learning, Notes on Intuitionistic Fuzzy Sets, 15(2), 33-36, (2009).

[6] E. Pap, Pseudo-analysis as a mathematical base for soft computing, Soft Computing, 1(2), 61-68, (1997).

[7] F. Altun, R. Şahin, C. Güler, Multi-criteria decision making approach based on PROMETHEE with probabilistic simplified neutrosophic sets, Soft Computing, 24(7), 4899-4915, (2020).

[8] F. Smarandache, Neutrosophy: neutrosophic probability, set, and logic: analytic synthesis & synthetic analysis, (1998).

[9] L.A. Zadeh, A note on Z-numbers, Information sciences, 181.14, 2923-2932, (2011).

[10] P. Patel, E.S. Khorasani, S. Rahimi, Modeling and implementation of Z-number, Soft Computing, 20, 1341-1364, (2016).

[11] B. Kang, Y. Deng, K. Hewage, R. Sadiq, A method of measuring uncertainty for Z-number, IEEE Transactions on Fuzzy Systems, 27(4), 731-738, (2018).

[12] S. Du, J. Ye, R. Yong, F. Zhang, Some aggregation operators of neutrosophic Z-numbers and their multicriteria decision making method, Complex & Intelligent Systems, 7, 429-438, (2021).

[13] J. Ye, Similarity measures based on the generalized distance of neutrosophic Z-number sets and their multi-attribute decision making method, Soft Computing, 25.22, 13975-13985 (2021).

[14] J. Fu, J. Ye, Simplified neutrosophic exponential similarity measures for the initial evaluation/diagnosis of benign prostatic hyperplasia symptoms, Symmetry, 9(8), 154, (2017).

DEPARTMENT OF MATHEMATICAL ENGINEERING, FACULTY OF ENGINEERING, GÜMÜŞHANE UNIVERSITY, GÜMÜŞHANE, TÜRKİYE
E-mail address: gulertugbagultekin@gmail.com

DEPARTMENT OF MATHEMATICS, FACULTY OF ARTS AND SCIENCES, RİZE, TÜRKİYE
E-mail address: elif.kirdag@erdogan.edu.tr

DEPARTMENT OF SOFTWARE ENGINEERING, FACULTY OF ENGINEERING, GÜMÜŞHANE UNIVERSITY, GÜMÜŞHANE, TÜRKİYE
E-mail address: mat.ridone@ gmail.com

IFSCOM-E 2024
10TH IFS AND CONTEMPORARY MATHEMATICS AND ENGINEERING CONFERENCE
04-07 SEPTEMBER 2024, MERSİN, TÜRKİYE
ISBN: 978-625-97923-1-6
pp: 70-76

DESIGN AND ELECTROMAGNETIC ANALYSIS OF MAGNETICALLY CONTROLLED SHUNT REACTOR

IRES ISKENDER and EMİR YÜKSELEN

0000-0003-1968-1857, 0000-0002-4364-9665

ABSTRACT
Today, the rate of utilization of renewable energy sources, which are abundant in nature, is increasing day by day. The energy obtained from these sources is generally converted into electrical energy and put into service for people. Today, smart electricity grids consist of an interconnected electrical system fed from many different energy sources. The performance of renewable energy systems is significantly affected by the power quality of the grid. Managing reactive power is very important for optimizing these networks. The demand for reactive power varies depending on the transmission line loads. In this context, there is increasing interest in using magnetically controlled reactors to address power quality issues. This study develops an analytical and equivalent model of a single-phase magnetically controlled reactor using a magnetic equivalent circuit. An electromagnetic simulation study is also conducted to validate the terminology used in the design process.

1. INTRODUCTION

Currently, most of the global energy demand is met by fossil fuels, which are finite resources expected to decline over time. Recently, renewable energy has emerged as a viable alternative. Renewable energy sources are abundant globally and have garnered significant attention in both research and practical applications. In large-scale renewable energy systems, maintaining power system quality, particularly addressing harmonics, is crucial for grid stability and safety. The proliferation of technological loads has exacerbated issues related to electricity quality, impacting the performance of end-user equipment. To mitigate these challenges, dynamic reactive power compensation and harmonic mitigation techniques have become increasingly essential. Traditional solutions such as synchronous capacitors and inductors have historically been employed to manage reactive power imbalance. However, Thyristor-based Static VAR Control (SVC) systems have gained prominence in recent years. These systems utilize Thyristor Controlled Reactors (TCRs) to provide or absorb reactive power as needed, with the inductance of Thyristor Controlled Shunt Reactors (TCSRs) adjusted via Thyristor control.

Date: September, 20, 2024.
Key words and phrases. Shunt reactor, Power factor, Magnetic field, Air-gap, Finite Element Method,

The application of such reactors is critical in high-power, high-voltage systems, although they entail significant costs. Alternatively, Magnetically Controlled Reactors (MCRs) or magnetically controllable shunt reactors (MCSRs) are widely adopted in high-voltage transmission lines.

In MCRs, the reactor's inductance can be adjusted by varying the magnetic flux through the core. The power factor of a line fluctuates with varying loads, necessitating corresponding adjustments in the reactor's reactance connected to the line. Magnetically controlled shunt reactors facilitate automatic management of the power system's reactive power and contribute to stabilizing voltage levels. To minimize the size of inductive reactors, air gaps are introduced into the core, underscoring the importance of optimizing air gap length during reactor design. Recent research has focused on exploring different control methods for shunt reactors [1-15].

This study aims to develop the equivalent circuit and electrical design for a single-phase magnetically controlled reactor rated between 10 to 12.5 kVar. The methodology involves obtaining the equivalent model of the reactor and subsequently comparing theoretical predictions with numerical results from a 3D simulation study to validate the design approach.

2. MATHEMATICAL MODEL OF THE REACTOR

This study focuses on adjusting the reactor's reactance by controlling the magnetic flux within its core. This method involves regulating the reactance by adjusting the current through a DC-fed winding. The primary objective of this paper is to achieve the design and implementation of a magnetically controlled reactor with adjustable power. Table 1 presents the technical specifications of the reactor under consideration.

Parameter	Value
Rated power	10-12.5 kVAr
Voltage	220 V
Phase	Single
Frequency	50 Hz

TABLE 1. Parameters of the reactor

Figure 1 illustrates the core's operation based on a typical B-H curve. In the absence of I_{dc} (DC current), the maximum flux occurs at point P1 on the B-H curve. As I_{dc} increases from zero, the maximum magnetic flux shifts to point P2 on the curve. Consequently, as the DC current varies, the operating point of the magnetic circuit moves along the B-H curve from P1 to P2. This shift in the circuit's operating point alters the reactor's inductance, thereby affecting its inductive power.

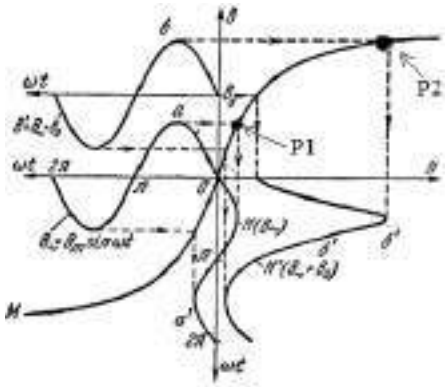

FIGURE 1. Operation principal of the core on typical B-H curve

Figure 2 depicts the B-H curve for an M4 core material with dimensions of 0.27 mm and a specific power loss of 1.1 W/kg. The curve demonstrates that as the current increases, the magnetic flux density (B) also increases. Consequently, the operating point of the reactor moves towards the saturation region.

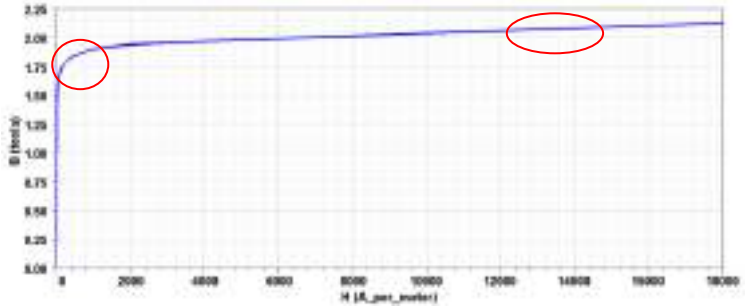

FIGURE 2. B-H curve of an M4 type core material

2.1. Calculation Based on the Minimum Power of the Reactor

In this scenario, the magnetic circuit operates within the linear region of the B-H curve. The magnetic flux density is set at 1.5 T for the purposes of this study. The initial design calculation steps are outlined below.

(2.1) $$Q = VI$$

(2.2) $$V = L\omega I$$

(2.3) $$L = \frac{220}{2\,\pi f \times 45.45} = 0.0154 = 15.4\ \text{mH}$$

(2.4) $$N = \left(\frac{B}{\mu_0 I}\right)L_g$$

(2.5) $$L = \left(\frac{N^2}{\mathcal{R}_g}\right) = \frac{B^2 L_g A}{\mu_0 I^2}$$

Assuming lg as 1.68 mm,

(2.6) $$A = 246\ \text{cm}^2$$

(2.7) $$NI = \emptyset\mathcal{R}_g = 26.73 \cong 27$$

(2.8) $$d = \sqrt{\frac{4\times A}{\pi \times 0.95}} \times 10 = 169.186\ mm$$

The DC winding turn number is considered as 1500 in this study.

3. SIMULATION STUDY

Ansys-FEM analysis was conducted using the initial design parameters. The reactance of the reactor is influenced by the length of the air gap. The air gap required to achieve a specific reactance may differ between theoretical and practical applications. Therefore, reactor design should consider the ratio between theoretical and practical approaches to achieve the desired reactance. Figure 3 illustrates the correlation between theoretical and practical air gap lengths to achieve identical reactance values.

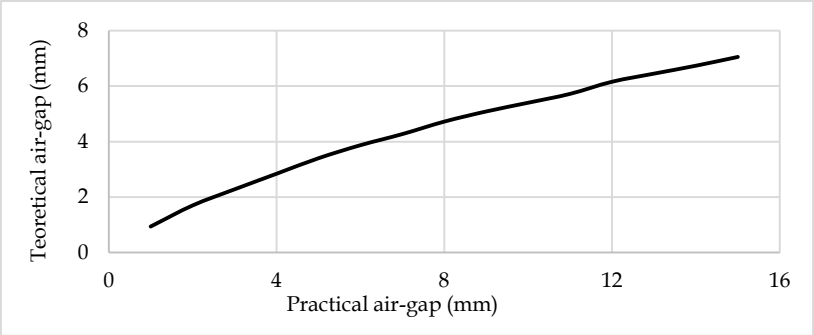

FIGURE 3. The relationship between the theoretical and practical air gap length [16]

Figure 4 illustrates a core with two windings: the inner winding powered by DC current and the outer winding by AC current or voltage. Simulation results depict parameter variations.

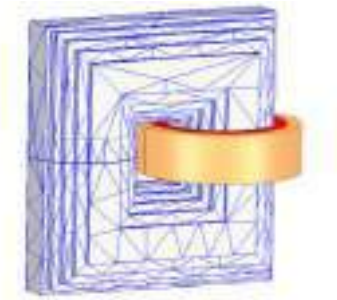

FIGURE 4. The reactor Ansys 3D model

Figure 5 displays that when the applied AC voltage is 222V rms and the DC current is set to zero, the ac current rms value is 45.77 A and the peak value of magnetic flux density is 1.52 T.

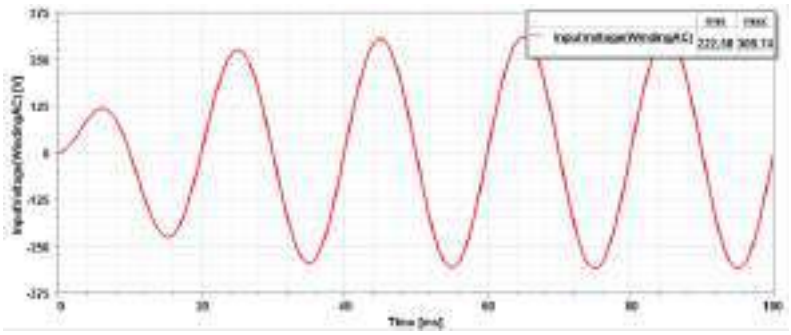

(a)

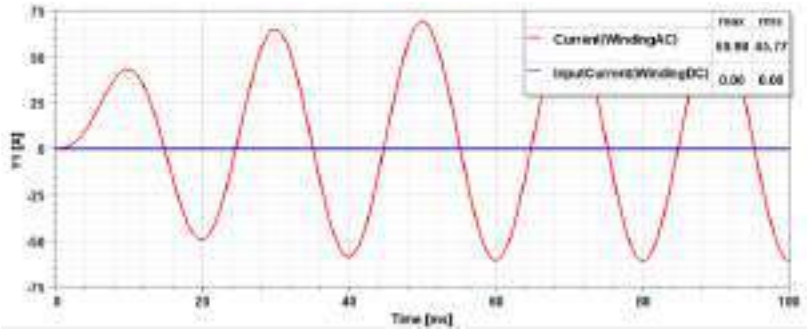

(b)

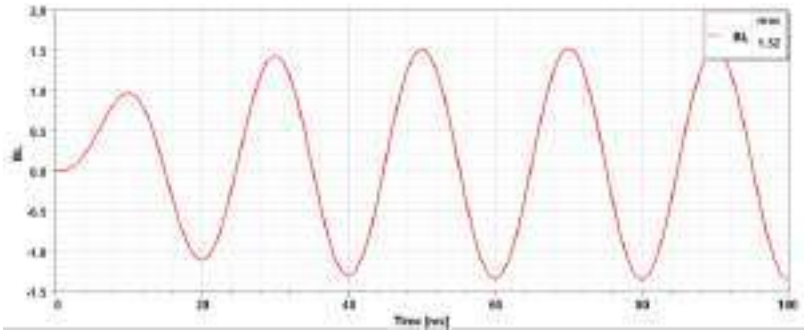

(c)

FIGURE 5. (a) Applied voltage, (b) I_{ac} current of the reactor, (c) change of magnetic flux

Figure 6 illustrates that when a DC current (I_{dc} = 0.3) is applied to the DC winding, the magnetic flux density (B) increases compared to the situation while there is not any DC current, causing the operating point of the magnetic circuit to shift towards the saturation region and this situation causes an increase in the reactive power of the reactor. In another simulation a voltage of 220 V rms is applied to the AC winding (outer winding) and the DC winding current (inner winding) is adjusted to 0.3 A. Figure 6 presents the results obtained from this simulation study.

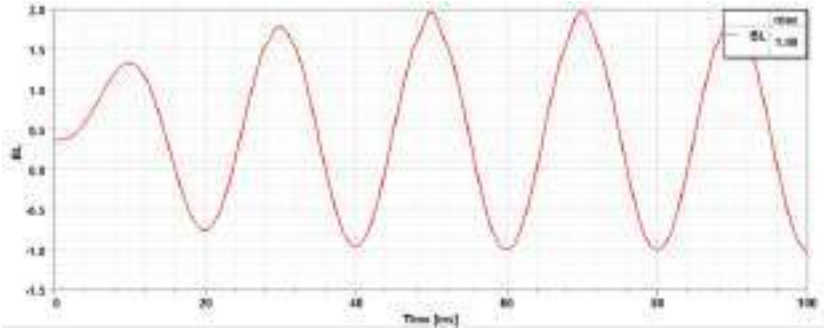

(a)

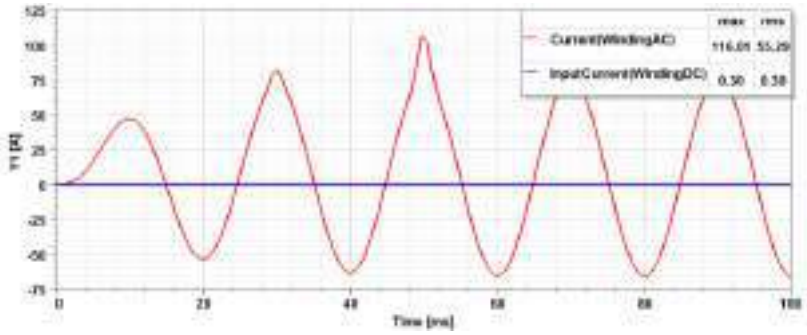

(b)

FIGURE 6. In the case of I_{dc} = 0.3 A, (a) change of B, (b) changes of I_{ac} and I_{dc}

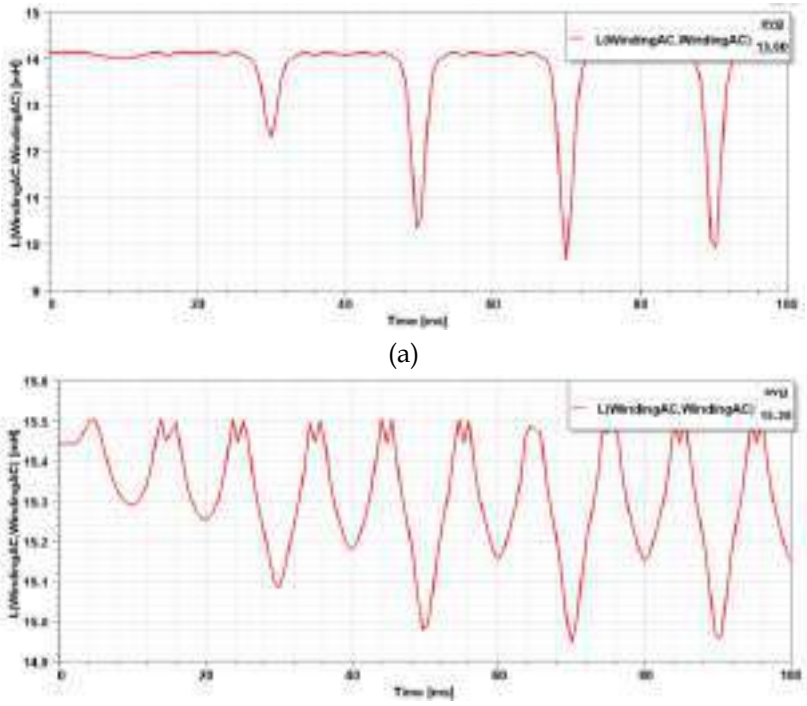

(a)

(b)

FIGURE 7. Inductance of the reactor, (a) with DC current, (b) without DC current

Figure 7 demonstrates the difference between the inductance value of the reactor for both conditions.

4. CONCLUSIONS

This paper includes a literature review aimed at developing the design concept for the reactor under consideration. Initial reactor design was conducted based on mathematical studies. Subsequently, Finite Element Method (FEM) analysis was performed on the preliminary design, confirming and supporting the mathematical expressions and design methodologies used. Identification of the impact of air gap length and cross-section on magnetic circuit parameters is carried out in this study as well.

The results of this study are expected to be useful in the design stage of reactor regarding to achieve both optimal performance and cost. Keeping the reactor design at a correct and safe level will be beneficial in improving the power quality of the grid.

NOMENCLATURES

Q: Reactive power of the reactor
L: Inductance of the reactor
I: Rated current of the reactor
N: Turn number of the specified winding
Lg: Air gap distance
$\mathcal{R}_g$: Reluctance airgap
A: Core cross section area
μ_0: Vacuum permeability in

REFERENCES

[1] H. Fathy, A. A. Awad, E. E. Mansour, Thyristor Controlled Reactor with Different Topologies Based on Fuzzy Logic Controller, International Journal of Engineering Research, 4(9), 498-505, (2015).
[2] S. Mahapatra, A. Goyal, N. Kapil, Thyristor Controlled Reactor for Power Factor Improvement, International Journal of Engineering Research and Applications, 4(4), 55-59, (2014).

[3] A. Nilakantan, V. Karsten, A. Krämer, Variable Active and Reactive Power Control Using OLTC In the Power Network, Article in Water and Energy International, (2019).
[4] H. M. Aung, Design of 25 MVA Shunt Reactor for 230 kV Transmission Line, International Journal of Scientific Engineering and Technology Research, 3(11), 2481-2486, (2014).
[5] S. W. Naing, Design and Simulation of 20 MVAR Three Phase Shunt Reactor for Voltage Suppression at 230 kV Transmission Line, International Journal for Innovative Research in Multidisciplinary Field, 5(1), 62-71, (2019).
[6] A. Lotfi, M. Faridi, Design Optimization of Gapped-Core Shunt Reactors, IEEE Transactions on Magnetics, 48(4), 1673-76, (2012).
[7] A. Moftah, Z. Rajab, I. Ighneiwa, Investigation in Thyristor- Controlled Reactor (TCR), Association for Computing Machinery, (2020).
[8] A. Lotfi, M. Faridi, Design optimization of gapped-core shunt reactors, IEEE Trans. Magn, 48, 1673–1676, (2012).
[9] A. Dönük, Optimum design of single and three phase iron core shunt reactors, Journal of the Faculty of Engineering and Architecture of Gazi University, 37(2), 1063-1076, (2022).
[10] A. Antonov, I. Kosolapov, M. Peshkov, Y. Goryushin, P. Bulykin, L. Kubarev et al., Fast response thyristor controlled shunt reactor, Development and application experience, CIGRE Session, 46, (2016).
[11] S. Bharti, S. P. Dubey, Controlled shunt reactor for UHVAC system reactive power control, Recent Adv. Electr. Electron. Eng., 13, 417–425, (2020).
[12] W. Zheng, Compound flexible control strategy for magnetically controlled shunt reactor suppressing overvoltage, Proceeding of the China International Conference on Electricity Distribution, 1–4, (2014).
[13] B. Bazilev, V. Bespalov, S. Dyagileva, P. Makarov, M. Makarova, B. Oleksyuk, Dual scheme based mathematical modeling of magnetically controlled shunt reactors 6–500 kV, Electric Power Quality and Supply Reliability, 1–4, (2012).
[14] M. Ebrahimi, R. Zeinali, H. Siahkali, A multi-objective model for allocation of Magnetically Controlled Shunt Reactors, 2015 IEEE 8th GCC Conference & Exhibition, 1–6, (2015).
[15] W. J. Zheng, X. Zhou, Adaptive tracking algorithm for magnetically controlled shunt reactor control.
[16] R. Jez, "Influence of the Distributed Air Gap on the Parameters of an Industrial Inductor," in IEEE Transactions on Magnetics, vol. 53, no. 11, pp. 1-5, Nov. 2017

DEPARTMENT OF ELECTRICAL AND ELECTRONICS ENGINEERING OF ÇANKAYA UNIVERSITY, ANKARA, TURKEY
E-mail address: ires@cankaya.edu.tr

DEPARTMENT OF ELECTRICAL AND ELECTRONICS ENGINEERING OF ÇANKAYA UNIVERSITY, ANKARA, TURKEY
E-mail address: emiryukselen@cankaya.edu.tr

IFSCOM-E 2024
10TH IFS AND CONTEMPORARY MATHEMATICS AND ENGINEERING CONFERENCE
04-07 SEPTEMBER 2024, MERSİN, TÜRKİYE
ISBN: 978-625-97923-1-6
pp: 77-86

NUMERICAL ANALYSIS OF A PHASE CHANGE MATERIAL-BASED THERMAL CONTROL SYSTEM FOR SMALL SATELLITES

BURAK İZGİ

0000-0001-9491-8653

ABSTRACT
In low Earth orbit, small satellites (SmallSats) face significant thermal management challenges. Throughout their orbit, they encounter two contrasting thermal conditions: extreme heat and extreme cold. Ensuring that small satellites operate within optimal temperature ranges is crucial for their reliable performance and durability. However, their compact size and restricted payload capacity present unique challenges in managing the thermal performance of electronics. This study presents the numerical analysis results of a PCM-based thermal control system for SmallSats. The investigation focuses on the impact of various PCM and fin materials on TCM performance. The results indicate that the base temperature of the TCM oscillates around the phase change temperature of the PCM during the orbital period. Among the PCMs studied, n-octadecane, n-eicosane, and hexadecane, the highest TCM base temperature of 36.92°C was observed with n-eicosane, while the lowest base temperature of 15.46°C was observed with hexadecane. These findings highlight the potential of PCM-based TCMs to enhance thermal management in small satellites, ensuring their efficient and reliable operation.

1. INTRODUCTION

Small satellites (SmallSats), due to their compact size and restricted payload capacity, pose distinct challenges in managing the thermal performance of electronic components [1], [2]. Ensuring that these devices operate within optimal temperature ranges is essential for their reliable performance and durability. SmallSats function in extreme environments where temperature fluctuations can greatly affect the performance and dependability of electronic systems. The thermal management task is further complicated by the cyclic operation of SmallSats, which involves repeated on-off cycles. Key challenges include constrained space, limited payload capacity, and the necessity for effective heat dissipation to avoid overheating of the devices [3].

Traditional thermal control in SmallSats uses passive methods [4] like radiative cooling

Date: September, 20, 2024.
Key words and phrases. Phase change materials, thermal management, small satellites.

and conductive heat transfer, which are limited by surface area and material properties, and active methods [5] like heat pipes [6] and thermoelectric coolers [7], which add complexity and require extra power [8]. Phase Change Materials (PCMs) provide a promising alternative by storing and releasing thermal energy during phase transitions, facilitating efficient heat transfer and nearly constant temperatures [9]. Elshaer et al. [10] examined the impact of PCM mixtures on satellite thermal management in an intermittent low Earth orbit environment. Their findings indicated that, unlike single PCM scenarios, the thermal performance of PCM combinations was largely unaffected by the heating load. Kansara et al[11] [12] conducted numerical studies to assess the effects of microgravity conditions and heat source orientation on a thermal control module for space applications. They found that reducing gravitational acceleration from g to g/80 resulted in an 18% decrease in the average liquid fraction. Wang [13] used numerical simulations to investigate methods for improving thermal conductivity in a tubular latent heat thermal energy storage system for microgravity spacecraft. By integrating metal foam with fins, a validated numerical model was created through experimental validation. The study showed that optimizing the coupling structure between metal foam and fins reduces melting time, enhances heat transfer efficiency with more fins, and decreases heat buildup in the system's upper section. Raj et al. [14] explored different fin configurations' effects on a solid-solid phase change material (SS-PCM) thermal control module for satellite avionics. Using numerical simulations and Taguchi optimization, they found that square straight fins provide better heat transfer and lower heat sink base temperatures than circular and triangular fins.

The aim of this study is to present the numerical analysis results of a PCM-based thermal control module (TCM) for small satellites. The study investigates the effects of different PCM and fin materials on TCM performance. By creating a CFD model to simulate the phase transition of an enclosed PCM, the study aims to understand the thermal management process during the cyclic operation of SmallSats.

2. METHOD

The thermal control method for electronic devices in SmallSats operates on a cyclic system, as shown in FIGURE 1. When the electronic device is active ("on" phase), it generates heat, which the PCM absorbs, causing a phase change. The PCM stores the excess heat as latent energy. During the "off" phase, this stored thermal energy is released from the PCM using radiators, heat pipes, or thermal straps, which help dissipate the heat and allow the PCM to refreeze. This cycle of melting and freezing enables the electronic device to maintain a relatively constant temperature during operation.

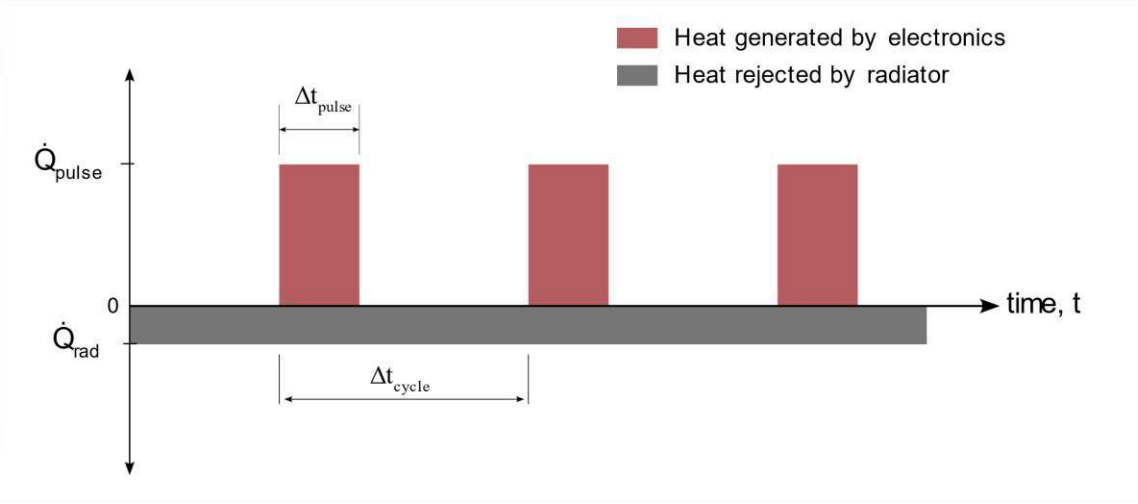

FIGURE 1. Cyclic operating electronic device (adapted from [15]).

The schematic view and dimensions of the thermal control device are shown in FIGURE 2. The device, measuring 104 x 104 x 30 mm, contains parallel fins, between which PCM is filled. The fins, container, and cover plate all have a thickness of 2 mm. The cover plate serves as a thermal radiator, emitting heat into outer space.

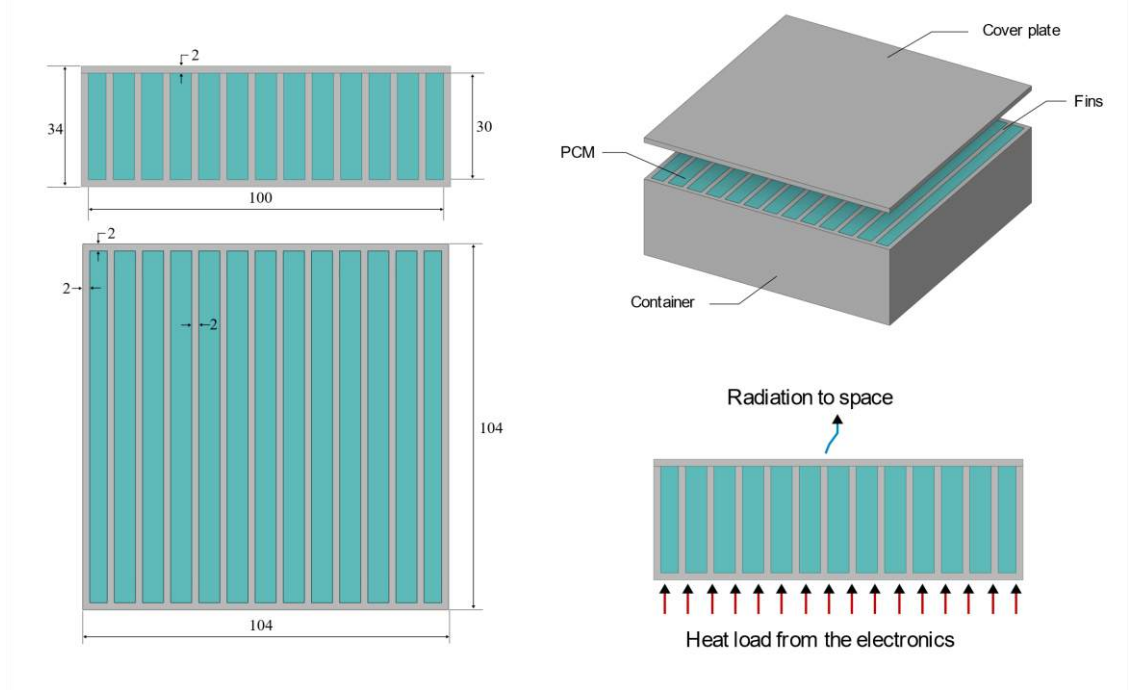

FIGURE 2. Schematic view and dimensions of the thermal control device.

A CFD model of an enclosed PCM was created to simulate its phase transition. This model utilized the enthalpy-porosity technique [16], [17] and was solved using the control volume method with the CFD software ANSYS Fluent. The assumptions underlying the numerical model are as follows:

- Since the microgravity environment, the natural convection in liquid PCM is neglected.
- PCM properties are assumed constant.
- During the phase change, the volume expansion is neglected.
- Direct-solar radiation and albedo effects are neglected.

The thermophysical properties of the PCMs and fin-container materials examined in this study are presented in the TABLE 1.

TABLE 1 Thermophysical properties of the PCMs and fin-container materials.

	ρ [kg/m³]	C_p [kJ/kg°C]	k [W/m°C]	L [kJ/kg]	T_m [°C]	Ref.
PCM						
n-octadecane	820.5	2.078	0.1624	242.454	28	[18]
n-eicosane	790	2.05	0.2735	237.4	36.7	[19]
Hexadecane	835	2.11	0.15	237.1	16.7	[11]
Fin-container						
Aluminum	2700	0.896	167	-	-	[19]
Copper	8978	0.381	387.6	-	-	[20]
Steel (carbon)	7854	0.434	60.5	-	-	[20]

Heat transfer in the TCM is mainly through conduction. Under microgravity conditions, natural convection effects are considered negligible, and thus, continuity and momentum equations are not applied. These simplifications allow for a significant reduction in computational time while maintaining the reliability of the results. The primary conduction heat transfer is modeled using a 3D heat conduction equation, as illustrated below:

$$\frac{\partial(H)}{\partial t} = \left(\frac{k}{\rho}\right)\nabla^2 \mathrm{T} \tag{1}$$

where the H, enthalpy of the PCM is the sum of sensible and latent enthalpies and defined as:

$$H = h_{ref} + \int_{T_{ref}}^{T} c_p dT + \varphi L \tag{2}$$

Here, L is the latent heat of the PCM, and φ denotes the liquid fraction. A linear relationship between temperature and the liquid fraction, φ, is defined within the temperature range where phase change occurs in the PCM:

$$\varphi = \begin{cases} 0 & T < T_s \\ \dfrac{T - T_s}{T_l - T_s} & T_s \le T \le T_l \\ 1 & T > T_l \end{cases} \tag{3}$$

In the TCM simulation cycle, the system experienced both heating and cooling phases. During the heating phase, the TCM was subjected to a varying heat load from satellite electronic components via the structure at the bottom plate (bottom wall). In the cooling phase, the TCM emitted thermal radiation into space continuously from the cover plate surface (top wall). The emissivity of top wall is 0.82. The side walls of the TCM were insulated. The boundary conditions are summarized in FIGURE 3.

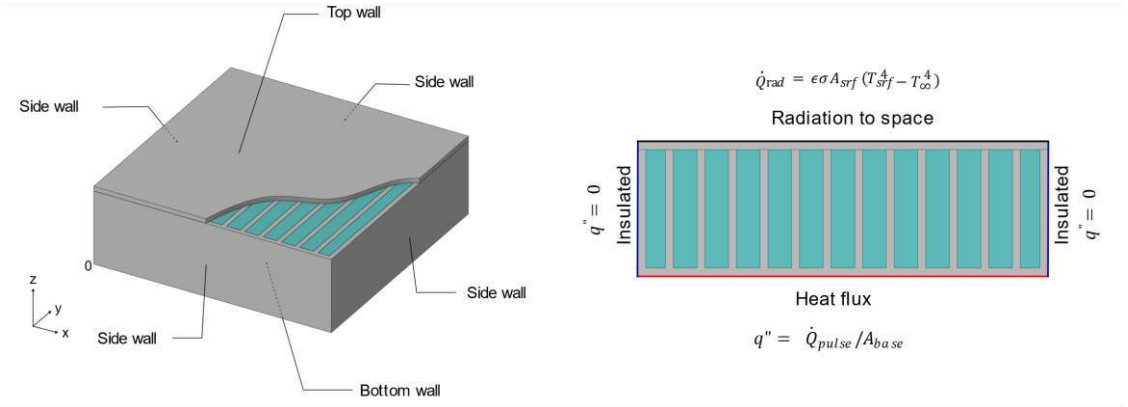

FIGURE 3. Boundary conditions.

The satellite's orbit period is 95 minutes, and the electronic component operates for 25 minutes in each orbit. The heat load of the electronic component is 15 W (FIGURE 4). The final steady-state temperature was independent of the initial temperature. Setting the starting temperature too high will just result in more cycles being required to reach equilibrium if the ultimate steady state is far from the starting point. Initial temperatures were chosen to minimize the time required to reach the final steady state.

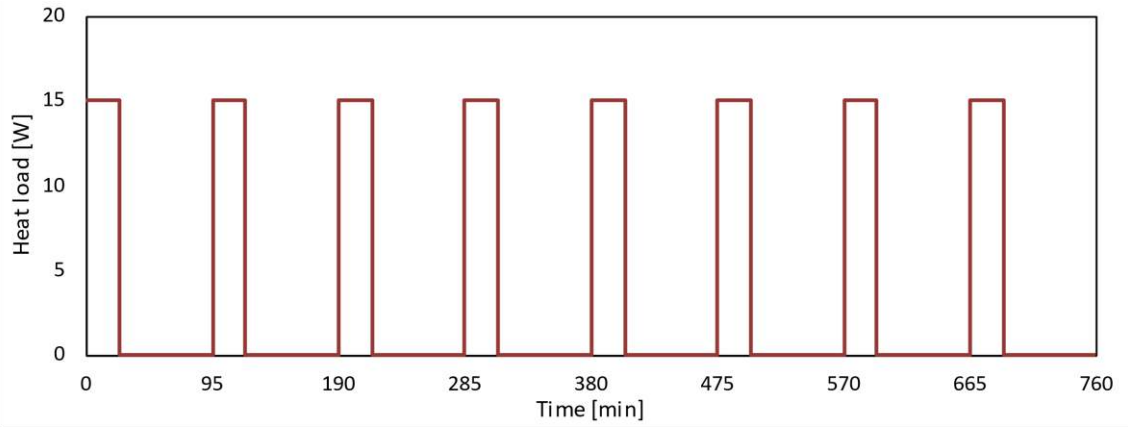

FIGURE 4. Change in heat load during the orbital cycle.

3. RESULTS AND DISCUSSION

In this study, the effects of three different PCMs and three different fin materials on the temperature of electronic components in the thermal control module of small satellites were analyzed. The parameters analyzed are presented in Table 2. In Cases 1, 2, and 3, the effects of using n-octadecane, n-eicosane, and hexadecane as PCMs were examined. In Cases 1, 4, and 5, the impact of using aluminum, copper, and steel as fin materials was analyzed. Case 6 investigated the case without fins, while Case 7 examined the scenario without PCM.

TABLE 2 Investigated cases.

Cases	PCM	Fin material	Container material
1	n-octadecane	Aluminum	Aluminum
2	n-eicosane	Aluminum	Aluminum
3	Hexadecane	Aluminum	Aluminum

4	n-octadecane	Copper	Copper
5	n-octadecane	Steel	Steel
6	n-octadecane	-	Aluminum
7	-	Aluminum	Aluminum

In FIGURE 5, the temperature variation of the bottom plate during the orbital cycle is presented for the finless case where the TCM is filled with n-octadecane PCM with a melting point of 28 °C. Because it offers information regarding the surface temperature of the satellite hardware, which is of interest, the bottom plate temperature is an important metric in assessing the thermal performance of the TCM during transient simulations. Therefore, the area-averaged temperature of the base plate in the TCM is presented. Until a stable state was reached, the model proceeded through multiple heat cycles. The base plate temperature's harmonic response is displayed in the temperature results during the course of the orbit.

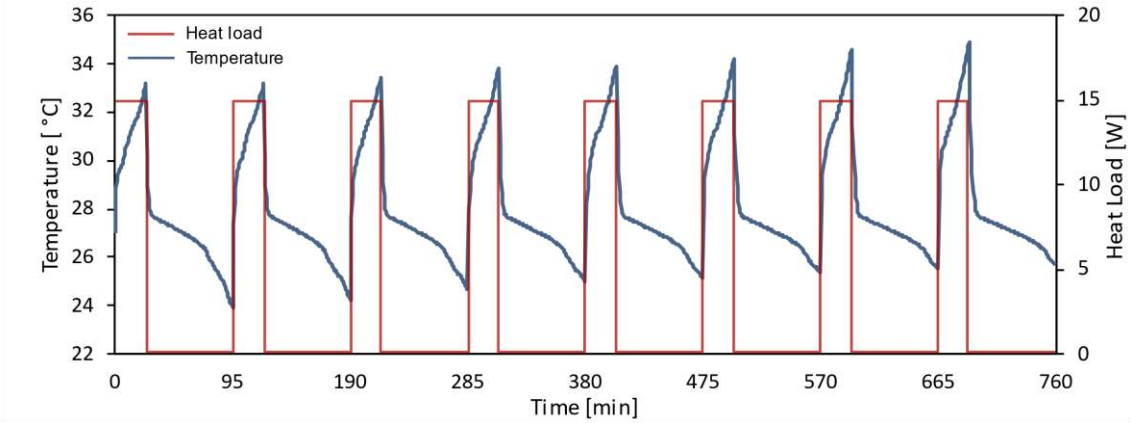

FIGURE 5 Change in bottom plate temperature and heat load during the orbital period.

In a steady state, the temperature oscillates between its minimum and maximum extremum points. Initially, the base plate temperature is below the PCM's melting point and rises sharply until it reaches this temperature. As melting begins, the rate of temperature increase slows, and the TCM stores heat during this process. When the heat flux from the electronics is turned off, the base plate temperature initially drops rapidly. Upon reaching the phase change temperature, the PCM starts to solidify, and the rate of temperature decrease slows down. During this process, the TCM releases the heat stored during melting back to the electronic component, preventing excessive cooling.

The effect of different PCMs on the base plate temperature is shown in FIGURE 6. Cases 1, 2, and 3 represent n-octadecane, n-eicosane, and hexadecane PCMs, respectively. As shown, the bottom plate temperature oscillates around the phase change points of the PCMs throughout the orbital period. For n-octadecane with a melting point of 28 °C (Case 1), the maximum base plate temperature is calculated as 28.46°C, and the minimum as 26.37°C. For n-eicosane with a melting point of 36.7°C (Case 2), the maximum and minimum base plate temperatures are 36.92°C and 32.87°C, respectively. For hexadecane with a melting point of 16.7°C (Case 3), the maximum and minimum base plate temperatures are calculated as 17.63°C and 15.46°C, respectively.

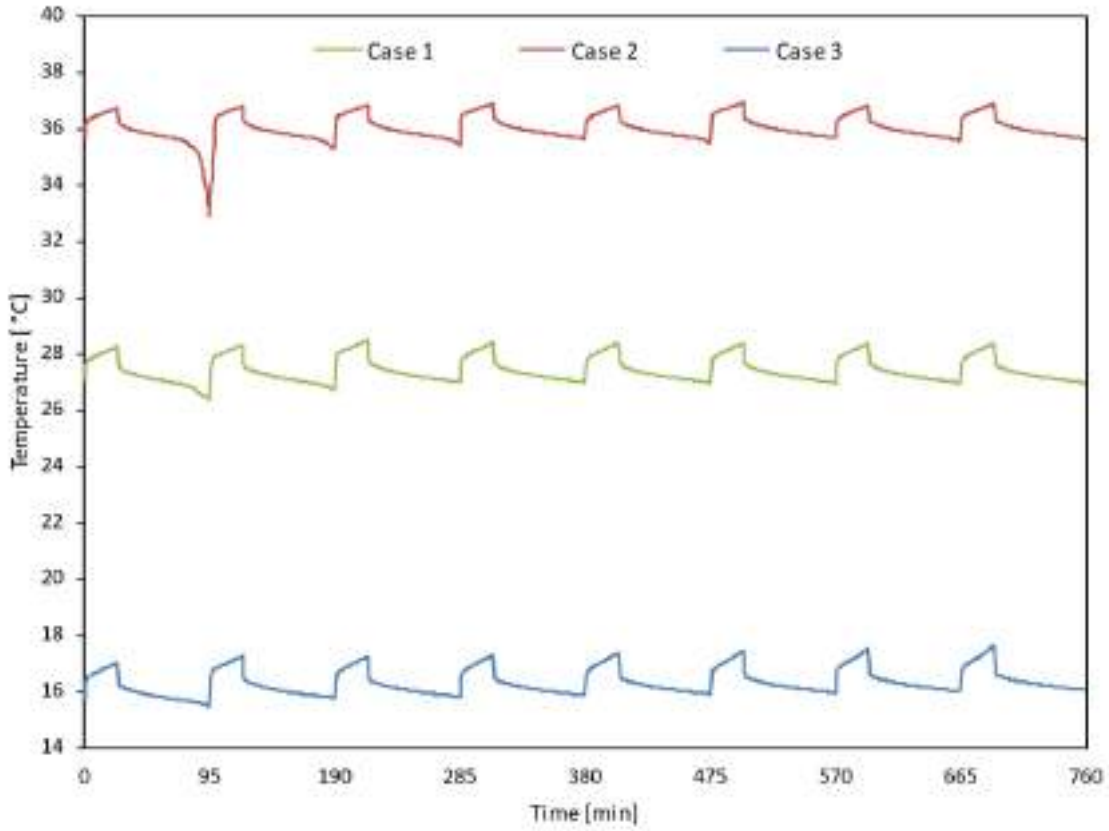

FIGURE 6 Change in bottom plate temperature during the orbital cycle for various PCMs.

The effect of fin material on the base plate temperature in the TCM is presented in FIGURE 7. Aluminum (Case 1), copper (Case 4), and steel (Case 5) were selected as fin materials. It is observed that the fin material has a no effect on the minimum base plate temperature but impacts the maximum temperature. The maximum base plate temperatures for aluminum, copper, and steel fins are calculated as 28.46°C, 28.22°C, and 29.10°C, respectively.

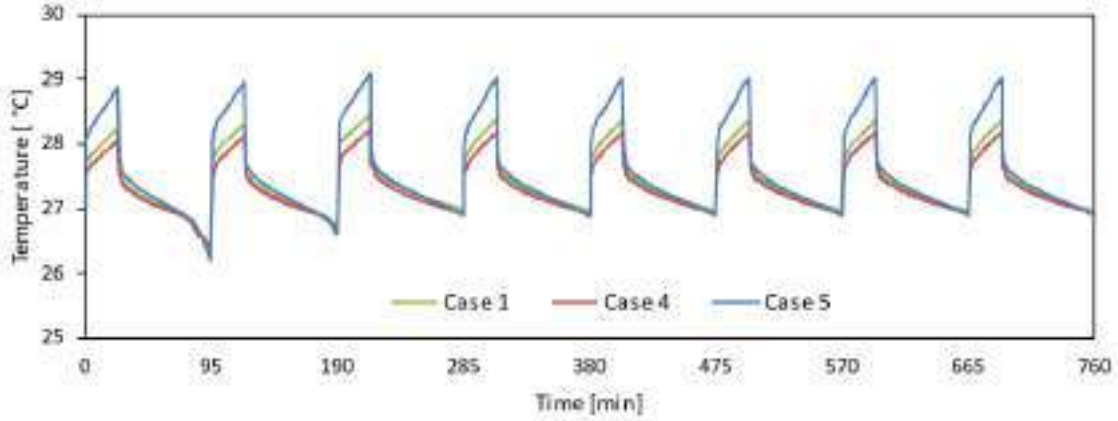

FIGURE 7 Change in bottom plate temperature during the orbital cycle for various fin materials.

FIGURE 8 compares the finless TCM completely filled with PCM (Case 6) to the finned TCM (Case 1). In the finless TCM, the maximum and minimum base plate temperatures are 34.91°C and 23.93°C, respectively, while in the finned case, these temperatures are 28.46°C and 26.37°C. The use of fins reduces the difference between maximum and minimum temperatures, allowing the electronic equipment to operate within a more stable temperature range. Specifically, the temperature difference is reduced by 76% when fins are used compared to the scenario without fins.

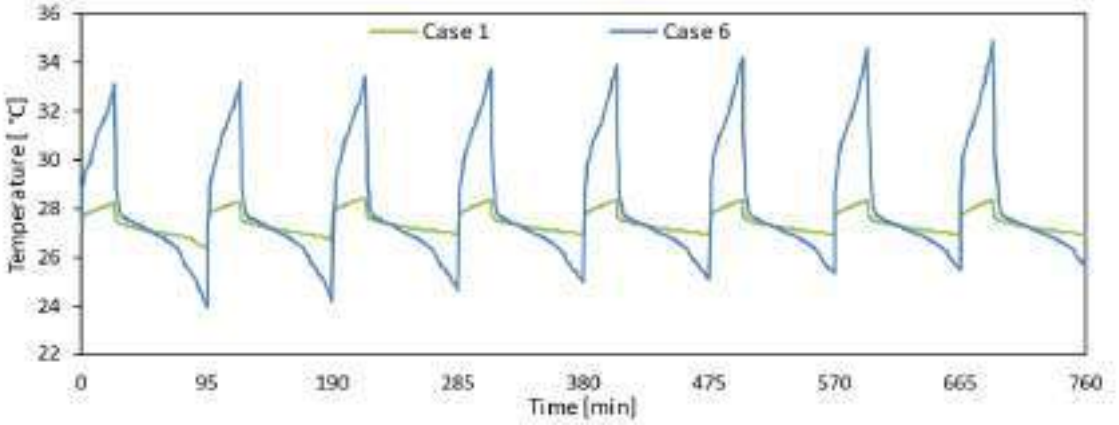

FIGURE 8 Variation in bottom plate temperature during the orbit cycle for finless and finned cases.

In the scenario where no PCM is used and the electronic component is directly connected to the radiator, the variation of the bottom plate temperature over the orbit cycle is compared with the PCM scenario in FIGURE 9. In this case, the TCM is assumed to be a solid aluminum block. The maximum base plate temperature is calculated as 32.87°C, and the minimum as 15.85°C, resulting in a temperature difference of 17.02°C. In the scenario using n-octadecane as PCM, the maximum and minimum base plate temperatures are 28.46°C and 26.37°C, respectively, with a temperature difference of 2.09°C. The use of PCM significantly reduces the temperature difference between maximum and minimum values.

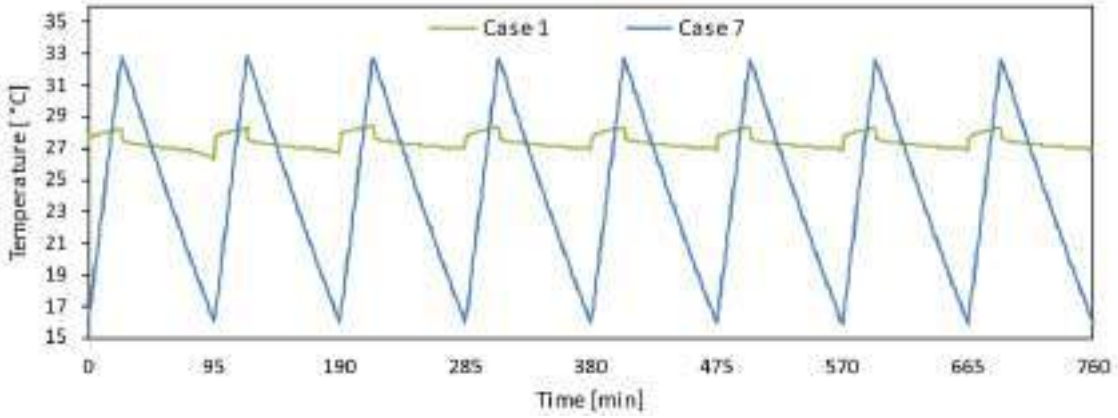

FIGURE 9 Variation in bottom plate temperature during the orbital period for PCM and no-PCM cases.

4. COCLUSIONS

In this study, the numerical analysis results of a PCM-based thermal control module for small satellites are presented. The effects of various PCM and fin materials on the TCM performance are investigated. The results can be summarized as follows:

- The base temperature of the thermal control module oscillates around the phase change temperature of the PCM during the orbital period. Among n-octadecane, n-eicosane, and hexadecane PCMs, the highest TCM base temperature of 36.92°C was observed with n-eicosane, while the lowest base temperature of 15.46°C was observed with hexadecane.
- As the heat transfer coefficient of the fin material increases, the maximum TCM base temperature decreases. When steel is used as the fin material, the maximum base

temperature is calculated as 29.1°C, whereas when copper is used, the maximum base temperature is calculated as 28.22°C.

- The difference between the maximum and minimum base plate temperatures of the TCM decreases when both PCM and fins are used together. In the scenario with only PCM, the temperature difference between the maximum and minimum values is calculated as 8.72°C. In the case of a solid aluminum TCM without PCM, this difference is 17.02°C. When both PCM and fins are used, the smallest temperature difference of 1.89°C is achieved in Case 4.

REFERENCES

[1] V. Baturkin, Micro-Satellites Thermal Control—Concepts and Components, Acta Astronautica, 56(1–2), 161–170, (2005). doi: 10.1016/j.actaastro.2004.09.003

[2] R. Osiander, S. L. Firebaugh, J. L. Champion, D. Farrar, and M. A. GarrisonDarrin, Microelectromechanical Devices for Satellite Thermal Control, IEEE Sensors J., 4(4), 525–531, (2004). doi: 10.1109/JSEN.2004.830297

[3] R. Kovács and V. Józsa, Thermal Analysis of the SMOG-1 PocketQube Satellite, Applied Thermal Engineering, 139, 506–513, (2018). doi: 10.1016/j.applthermaleng.2018.05.020

[4] S. Tachikawa, H. Nagano, A. Ohnishi, and Y. Nagasaka, Advanced Passive Thermal Control Materials and Devices for Spacecraft: A Review, Int J Thermophys, 43(6), 91(2022). doi: 10.1007/s10765-022-03010-3

[5] J. Wang, Y. Li, X. Liu, C. Shen, H. Zhang, and K. Xiong, Recent Active Thermal Management Technologies for the Development of Energy-Optimized Aerospace Vehicles in China, Chinese Journal of Aeronautics, 34(2), 1–27, (2021). doi: 10.1016/j.cja.2020.06.021

[6] Q. Meng et al., Experimental Study on the Transient Behaviors of Mechanically Pumped Two-Phase Loop With a Novel Accumulator for Thermal Control of Space Camera Payload, Applied Thermal Engineering, 179, 115714, (2020). doi: 10.1016/j.applthermaleng.2020.115714

[7] V. K. Singh et al., Thermoelectric Cooler (TEC) Based Thermal Control System for Space Applications: Numerical Study, Applied Thermal Engineering, 224, 120101 (2023). doi: 10.1016/j.applthermaleng.2023.120101

[8] J. Chen, L. Liu, W. Xu, X. Huang, and H. Sheng, Design and Analysis of a Hollow Metallic Microlattice Active Cooling System for Microsatellites, Nanomaterials, 12(9), 1485(2022). doi: 10.3390/nano12091485

[9] Y. Huang, A. Stonehouse, and C. Abeykoon, Encapsulation Methods for Phase Change Materials – A Critical Review, International Journal of Heat and Mass Transfer, 200, 123458(2023). doi: 10.1016/j.ijheatmasstransfer.2022.123458

[10] A. M. Elshaer, A. M. A. Soliman, M. Kassab, and A. A. Hawwash, The Effect of Melting Point and Combination of Phase Change Materials on the Thermal Control Performance of Small Satellites in the Thermal Environment of Low Earth Orbit: Numerical Study, Journal of Energy Storage, 59, 106531(2023). doi: 10.1016/j.est.2022.106531

[11] K. Kansara, V. K. Singh, R. Patel, R. R. Bhavsar, and A. P. Vora, Numerical Investigations of Phase Change Material (PCM) Based Thermal Control Module (TCM) Under The Influence Of Low Gravity Environment, International Journal of Heat and Mass Transfer, 167, 120811(2021). doi: 10.1016/j.ijheatmasstransfer.2020.120811

[12] K. Kansara and V. K. Singh, Effect of heat source direction on the thermal performance of phase change material (PCM) based thermal control module (TCM) under the influence of low gravity environment', International Communications in Heat and Mass Transfer, vol. 128, p. 105615, Nov. 2021, doi: 10.1016/j.icheatmasstransfer.2021.105615.

[13] S. Wang, X. Hou, J. Yin, Y. Xing, and Z. Wang, Comparative Study of The Thermal Enhancement for Spacecraft PCM Thermal Energy Storage Units, Aerospace, 9(11), 705(2022). doi: 10.3390/aerospace9110705

[14] C. R. Raj, S. Suresh, R. R. Bhavsar, V. K. Singh, and K. A. Govind, Influence of Fin Configurations In The Heat Transfer Effectiveness of Solid Solid PCM Based Thermal Control Module for Satellite Avionics: Numerical Simulations, Journal of Energy Storage, 29, 101332(2020). doi: 10.1016/j.est.2020.101332

[15] D. Gilmore, Spacecraft Thermal Control Handbook, Volume I: Fundamental Technologies. Washington, DC: American Institute of Aeronautics and Astronautics, Inc.,(2002). doi: 10.2514/4.989117

[16] A. D. Brent, V. R. Voller, and K. J. Reid, Enthalpy-Porosity Technique for Modeling Convection-Diffusion Phase Change: Application to the Melting of a Pure Metal, Numerical Heat Transfer, 13(3), 297–318, (1988). doi: 10.1080/10407788808913615
[17] V. R. Voller and C. Prakash, A Fixed Grid Numerical Modelling Methodology for Convection-Diffusion Mushy Region Phase-Change Problems, International Journal of Heat and Mass Transfer, 30(8), 1709–1719, (1987). doi: 10.1016/0017-9310(87)90317-6
[18] J. Vogel and A. Thess, Validation of a Numerical Model With a Benchmark Experiment for Melting Governed By Natural Convection In Latent Thermal Energy Storage, Applied Thermal Engineering, 148, 147–159, (2019). doi: 10.1016/j.applthermaleng.2018.11.032
[19] C. H. Wang, M. H. Chen, J. D. Huang, and C. R. Chen, A Numerical Study of the Thermal Critical Component on FORMOSAT-7 with Phase Change Material', AMR, 1016, 764–768, (2014). doi: 10.4028/www.scientific.net/AMR.1016.764
[20] L.-L. Tian, X. Liu, S. Chen, and Z.-G. Shen, Effect of Fin Material on PCM Melting in a Rectangular Enclosure, Applied Thermal Engineering, 167, 114764, (2020). doi: 10.1016/j.applthermaleng.2019.114764.

DEPARTMENT OF MECHANICAL ENGINEERING, FACULTY OF ENGINEERING AND ARCHITECTURE, YOZGAT BOZOK UNIVERSITY, YOZGAT, TÜRKİYE
E-mail address: burak.izgi@bozok.edu.tr

IFSCOM-E 2024
10TH IFS AND CONTEMPORARY MATHEMATICS AND ENGINEERING CONFERENCE
04-07 SEPTEMBER 2024, MERSİN, TÜRKİYE
ISBN: 978-625-97923-1-6
pp: 87-96

THE EFFECT OF THE USE OF PARAFFIN WAX ON THE REGRESSION RATE OF HYBRID ROCKET ENGINES: A REVIEW

SÜREYYA SEVİNÇ VAROL, BİLGE ALBAYRAK ÇEPER and NAFİZ KAHRAMAN

0009-0002-0991-8494, 0000-0001-5556-5170 and 0000-0002-8698-8632

ABSTRACT

In this study, studies on the effect of the use of paraffin wax on the regression rate in Hybrid Rocket Engines (HRE) were compiled. Many studies have been conducted to prove that the use of liquefying fuels in HREs, which cannot be widely used due to low regression rates, has a positive effect on the regression rate. Paraffin wax, which is included in the thermoplastic fuels class, is often preferred among sustainable fuels because it is an easy material to recycle. It has been determined by studies that the use of paraffin wax, which is preferred as a liquefying fuel for attractive reasons such as low environmental impact and low cost, increases droplet drift in HRE and improves the regression rate. This review is intended to contribute to future studies.

1. INTRODUCTION

Hybrid rocket engines have been a popular field of study from the 1970s to the present [1]. Although there are many studies in this field in the literature, HREs, which have a low regression rate compared to solid and liquid-fueled rocket engines, have a limited field of use [2]. The studies carried out to eliminate this disadvantage include the addition of various additives [3,4,5], the use of fuel grains in different ports or lengths [6, 7, 8] and different additive manufacturing methods [9, 10]. Among the studies, the use of plastic (polyethylene [11], polypropylene [12] and paraffin wax [13, 14]) and organic (bio-polyethylene, bio-pp, bio-pu and wax [15]) fuels to achieve a high regression rate occupies a significant place in the literature. In particular, the increase in emission rates has pushed the field of rocket technology to look for more environmentally friendly solutions, as in many areas [16, 17, 18]. Recycling and reuse of plastics, research on new types of organic fuels, and studies on the production of synthetically low-emission fuels are some of the solutions found [15].

Date: September, 20, 2024.
Key words and phrases. Hybrid Rocket Engines, Paraffin Wax, Regression Rate.

Although paraffin wax, which is preferred due to its low emission rate, does not achieve efficient results when used alone, it can achieve high regression rates when used with different fuels [19]. It has been observed that paraffin-based fuels used as liquefying fuels increase the rate of regression [20]. Liquefying fuels form a liquid layer on the combustion surface and cause fuel droplets to drift in the direction of flow. This situation contributes to an increase in the regression rate. Paraffin wax is often used as a liquefying fuel because it provides a greater increase in the rate of regression compared to other fuels [21]. Studies on the positive effect of paraffin wax contained in thermoplastic fuels on the regression rate in HREs are available in the literature [15]. Most of the experimental studies have also been supported by numerical analyses [22, 23, 24]. Experimental studies have mainly been carried out on laboratory-scale hybrid rocket engines [25, 26, 27]. When we look at the literature, there are studies in which oxidizers such as GOX [26], LOX [28], N2O [29] and H2O2 [30, 31] are used as oxidizers in HRE.

This study aims to create an infrastructure for future studies by examining the effect of paraffin wax on the rate of regression in hybrid rocket engines. It is expected that the compilation of the causes related to the positive effect on the regression rate of paraffin wax used in fuel grains will increase the effectiveness of the studies to be conducted.

2. LITERATURE REVIEW

Gallo et al. [32] conducted an experimental study on the conditions affecting the regression rate in HRE. In the study, three fuel grains with different lengths (70 mm, 130 mm, 220 mm) were prepared. The effect of the fuel grain length on the regression rate was investigated using gaseous oxygen and paraffin wax-based fuel. In addition, the issues of propellant mixing and combustion instability were also discussed in the study. In order to support the experimental study, the simulation performed on the computational fluid dynamics (CFD) model provided information about the fluid field located in the combustion chamber. The findings obtained as a result of the study;

- The characteristic speed varies depending on the grain length.
- The regression rate depends on the axially increasing fuel grain consumption. However, the regression rate for the upstream region in all configurations shows a similar trend.
- It was found that the drift was not affected by the gas density.
- It was observed that all configurations (especially the 130 mm configuration) were affected by coarse combustion.

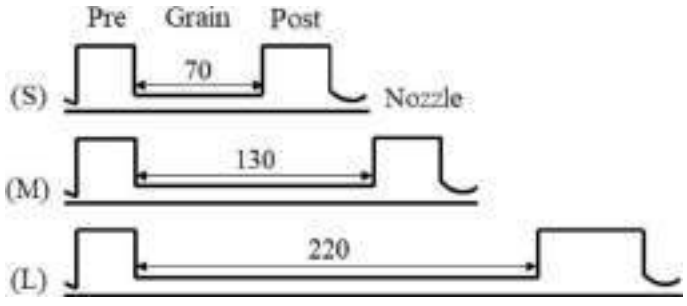

FIGURE 1. S, M and L Motor Types [32]

Tests performed on fuel grains are named as S, M and L in FIGURE 1. Here, S represents the tests performed on a 70 mm fuel grain; M represents the tests performed on a 130 mm fuel grain; L

represents the tests performed on a 220 mm fuel grain. The oxidizer-regression ratio graph depending on the test results is given in Figure 2.

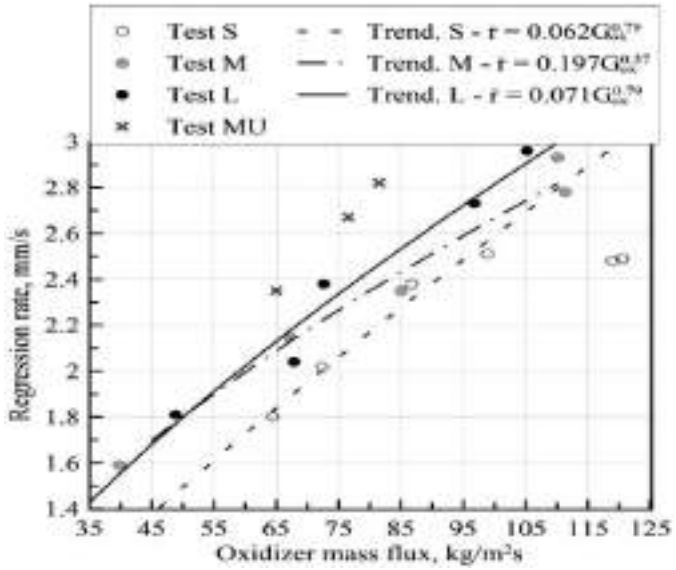

FIGURE 2. Oxidizer-Regression Rate Graph of S, L, M, MU tests [32].

Wu et al. [33] in their experimental study, they manufactured fuel configurations using paraffin wax and different polymer materials as a skeletal structure. Figure 3 shows a paraffin-polymer structure using ABS as the skeletal structure.Paraffin fuel cannot meet the necessary requirements when used alone due to its low mechanical strength. The use of polymer materials as the skeletal structure of fuel configurations is effective in strengthening the mechanical properties and achieving a high rate of regression. Various tests were carried out on the manufactured configurations. As a result of the tests conducted, it has been determined that the flame propagation rate of the configuration resulting from the production of ABS polymer reinforcement using the SLS technique is higher than that of other production techniques. A higher regression rate and better mixing efficiency have been observed in this new fuel. Therefore, it has been found that the new fuel has a higher combustion efficiency.

FIGURE 3. (a) Cross-section of Star-shape skeleton additived paraffin-wax fuel grain. (b) Isometric view of Star-shape skeleton. (c) Paraffin-wax and ABS Combination [33].

Thomas et al. [34] in their study, HTPB (hydroxyl-terminated polybutadiene) samples containing paraffin (pure HTPB, pure paraffin, molten macrocrystalline paraffin (10-75%) and solid microcrystalline paraffin (10-60%) fragments) were produced in different structures. Schematic representations of the movements are given in Figure 4. Also, Figure 5 shows the change in the regression rate depending on the oxidizing mass of pure htpb and htpb-pp mixtures at different ratios. The samples were burned in a HRE in a laboratory environment. HTPB with the addition of

macrocrystalline paraffin showed a 300% regression rate increase compared to plain HTPB. On the other hand, there was no significant increase in the regression rates of other mixtures. As a result of the study, it was not found appropriate to add paraffin to HTPB to adapt the combustion behavior in HREs and alternative methods were given.

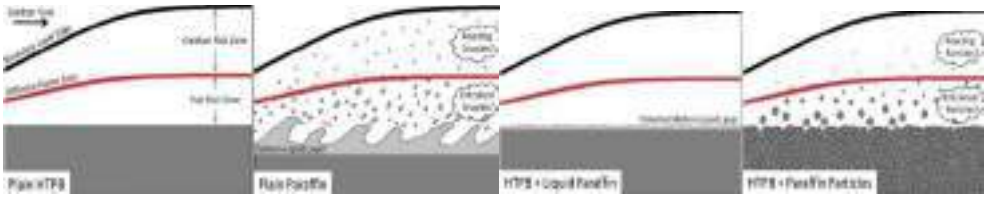

FIGURE 4. Schematics of four Fuel Mixtures [34].

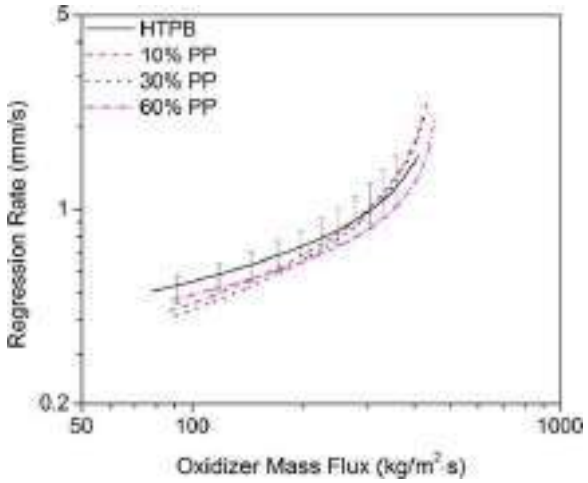

FIGURE 5. Oxidizer Mass Flux vs Regression Rate of HTPB and Paraffin Partical at different ratios [34].

Oztan et al. [35] in their study, they examined a composite fuel grain consisting of ABS and paraffin. A new configuration has been created by 3D printing with the addition of carbon dots (CDs) to the paraffin (1% by mass). A pure paraffin-ABS configuration was also produced using the 3D printing method for control purposes. The cross-sectional images of the created models are shown in Figure 6. The combustion performance of the produced samples was examined in the test assembly using gaseous oxygen. As a result of the study, an increase of 8.5% and 11% in the combustion efficiency of the CDs-added configuration compared to the pure paraffin-ABS configuration was observed, and a regression rate of 1.29 mm/sec was determined. The regression ratio graph related to fuel mixtures is shown in Figure 7.

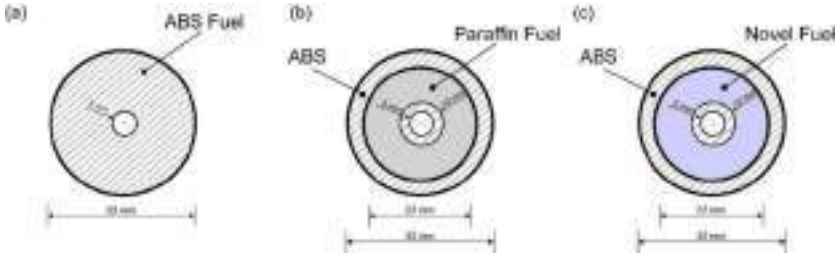

FIGURE 6. Cross-sectional dimensions of each fuel grain: (a) ABS; (b) ABS-pure paraffin; (c) CD-doped novel fuel [35].

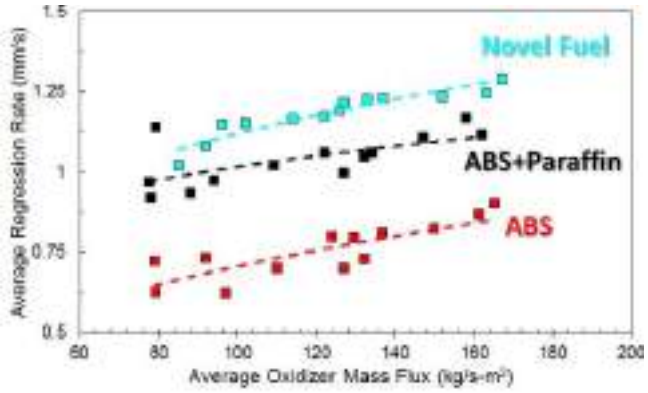

FIGURE 7. Correlation of ABS, ABS & Paraffin and Novel fuel [35].

Liu et al. [36] evaluated the regression rate of paraffin-based fuels using nitrous oxide (N2O) and gaseous oxygen (GOX) as oxidizers in their study. In the study, 38% solid paraffin, 28% liquid paraffin, 4% improved PE, 15% HTPB, 10% aluminum particle with a size of 10 μm and 15% magnesium particle with a size of 1 μm were used as the basic formulation. Catocene, copper chromite and cobalt stearate of 1% by weight were used as combustion catalysts. As a result of the study, it was found that both copper chromite and cobalt stearate increased the regression rate. In addition, it has been observed that the chamber pressure increases slightly more when using GOX compared to using N2O, so there is an increase in the regression rate. The regression rate change according to the oxidizer type is given in Figure 8.

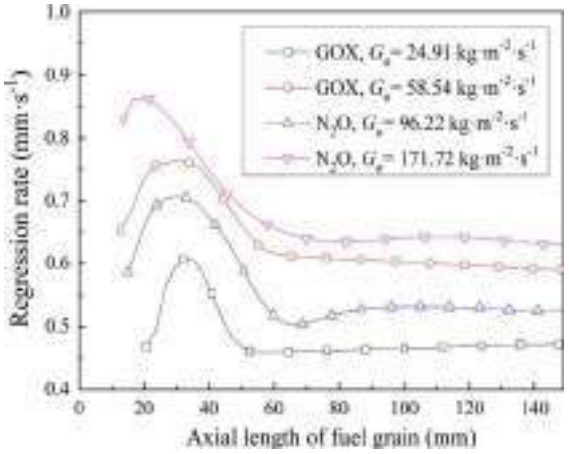

FIGURE 8. Length of fuel grain-regression rate curve by oxidizer types [36].

Migliorino et al. [37] performed experimental and numerical analyses on a HRE in their study. Paraffin wax and GOX were used in the experimental study. The regression rates were obtained by an

optical method. Regression rates in the between 0.5-2.5 mm/s range were obtained in the study examining the effect of vortex injection on regression rate. The regression ratio graph according to the different side room radius ratios is given in Figure 9. At the end of the study, it was found that the average regression rate depends on the oxidizer mass flow and the number of vortices, and a law was developed in this direction.

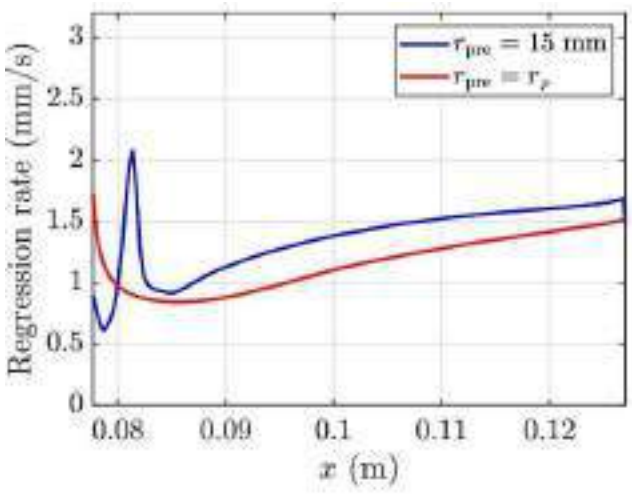

FIGURE 9. Regression rate curve of different prechamber radiuses [37].

Jamil et al. [38] proposed a new fuel composition containing metal additives in their study. High entropy alloys (HEA) were used as additives. The mixture ratios used are given in Table 1. Various tests and analyses were carried out on the new configuration. As a result of the analyses, it was found that the configuration with a high entropy alloy added achieved 86.92% more energy release compared to pure paraffin-based fuel. It is thought that this released energy will contribute to increasing the rate of regression. In light of the obtained data, it has been concluded that HEAs can be used in HREs in the future.

Fuel Sample	**Material (% weight)**	
	Paraffin Wax	**Additives**
Pure Paraffin Wax	100%	-
Paraffin Wax/HEA1	80%	20%
Paraffin Wax/HEA2	80%	20%
Paraffin Wax/Fe	80%	20%
Paraffin Wax/B	80%	20%
Paraffin Wax/Al	80%	20%

TABLE 1. mixing ratio of fuel configurations [38].

Pal et al. [39] in their study, they examined the fuel combustion performance in HRE. In the study, MgB_2 and CB (carbon black) substances were added to the paraffin-based fuel as additives. The combustion test of the mixture is given in Figure 10. The thermal stability of the new fuel configurations was examined. As a result of the tests, it was found that the regression rates of MgB_2 and CB reinforced fuels increased by 52% and 32% respectively. The findings obtained at the end of the study:

- The addition of MgB_2 to the fuel had a positive effect on its ultimate strength and modulus of elasticity.
- The addition of CB has a positive effect on thermal stability.

- The addition of CB and MgB_2 to thuel was found to increase the regression rate by 32% and 52%, respectively, compared to pure paraffin-based fuel. The regression ratio graph of the fuel configurations is given in Figure 11.
- The characteristic speed efficiency obtained as a result of the measurements has been found to have comparable values in HRE applications.
- As a result of the study, a MgB_2 combustion model proposal was given.

(a) (b)

FIGURE 10. (a) Combustion test of pure paraffin and (b) combustion test of P-CB-MgB_2 [39].

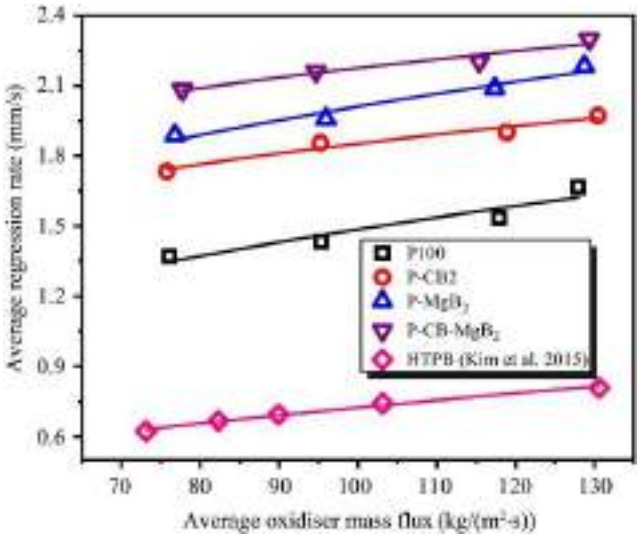

FIGURE 11. Regression rate change of fuel mixtures [39].

3. CONCLUSION

In the literature review, studies using paraffin wax were compiled. The studies examined are carried out in laboratory scale hybrid rocket engines. In the studies, different production methods, different additives and different oxidizers were used to examine the changes in regression rates. Thomas et al. (2021) showed that the addition of additives to paraffin increased the regression rate by 300%. In the study of Pal et al. (2023), it was observed that among the additives used, MgB2 increased the regression rate more than the other additives with an increase rate of 52%. Liu et al. (2020), who studied the effect of oxidizer type on paraffin-based fuel, found that gaseous oxygen increased the

regression rate more than nitrous oxide. Wu et al. (2022) compared SLS and SLA methods in their study. As a result of the study, it was observed that the SLS method has a surface roughness of 0.35 µm and the high spreading rate has a positive effect on the regression rate. These conclusions are planned to be a basis for the choice of fuel grain production method and the use of additives in future studies.

4. REFERENCES

[1] A. Hakobyan, H. Kocharyan, Hybrid Rocket Engine Optimization by Controlled Oxidizer Flow Dynamics, Aerospace Science and Technology, 153, (2024).

[2] S.-S. Wei, M.-C. Lee, J.-W. Huang, Y. Lu, C.-H. Kang, S.-T. Kao, S.-J. Lu, C.-H. Huang, J.-J. Zhan, Z.-R. Chen, A. Wang, T. H. Chou, A. Lai, Y. Lee, M.-T. Ho, H.-P. Lin, J.-S. Wu, Demonstration of Tethered Hovering Flight of HTTP-3AT Hybrid Rocket, Acta Astronautica, 191, 279-292, (2022).

[3] N. K. Madhusudhan, G. Micklow, Numerical and Thermochemical Analysis of Hybrid Rocket Fuels with Metallic Additives, Multidisciplinary Engineering Science and Technology, 7(11), (2020).

[4] N. A. B. M. Jamil, A. H. B. Mohamaddiah, M. H. B. Azami, N. H. Nordin, High Entropy Alloy as Metal Additive for Hybrid Rocket Propellant, Materialstoday: Proceedings, 75(1), 140-146, (2023).

[5] I. I. Ismail, N. H. Nordin, M. H. Azami, N. A. Abdullah, Metals and Alloys Additives as Enhancer for Rocket Propulsion: A Review, Journal of Advanced Research in Fluid Mechanics and Thermal Sciences, 90(1), 1-9, (2022).

[6] Z. Wang, X. Lin, F. Li, X. Yu, Combustion Performance of a Novel Hybrid Rocket Fuel Grain with a Nested Helical Structure, Aerospace Science and Technology, 97, (2020).

[7] Y. Funami, K. Uchishima, S. Homme, S. Nishino, A. Takano, Evaluation of Hybrid Rocket Fuel Grain with a Star Fractal Port Using Combustion Experiments, The Japan Society for Aeronautical and Space Sciences, 19(3), 295-303, (2021).

[8] T. Wei, G. Cai, H. Tian, X. Jiang, Experiment and Numerical Research on Regression Rate of Hybrid Rocket Motor with Single-port Wagon Wheel Fuel Grain, Acta Astronautica, 207, 265-282, (2023).

[9] H. Bikas, P. Stavropoulos, G. Chryssolouris, Additive Manufacturing Methods and Modelling Approaches: A Critical Review, Advanced Manufacturing Technology, 83, 389-405, (2016).

[10] C. Y. Yap, C. K. Chua, Z. L. Dong, Z. H. Liu, D. Q. Zhang, L. E. Loh, S. L. Sing, Review of Selective Laser Melting: Materials and Applications, Applied Physics Reviews, 2(4), (2015).

[11] T. Guang, T. Hui, J. Xianzhu, C. Ruikai, L. Yudong, Z. Yuanjun, Experimental Study on Precise Thrust Control of Hydrogen Peroxide and Polyethylene Hybrid Rocket Motors, Acta Astronautica, 196, 303-313, (2022).

[12] M.-C. Li, S.-S. Wei, C.-H. Hung, J.-S. Wu, Experimental and Numerical Investigation of Swirling H2O2 and Polypropylene Hybrid Rocket Motor with Regenerative Cooling, Acta Astronautica, 190, 283-298, (2022).

[13] S. Srivastava, A. K. Thakur, Comparison of Propellant Characteristics Using Paraffin and Blends of Aluminum and Magnesium with Oxidizers in Hybrid Rocket Engine, Aerospace Systems, 6, 119–128, (2023).

[14] G. Cican, A. Paraschiv, A. N. Buturache, A. I. Hapenciuc, A. Mitrache, T.-F. Frigioescu, Experimental Research into an Innovative Green Propellant Based on Paraffin–Stearic Acid and Coal for Hybrid Rocket Engines, Inventions, 9(2), 26, (2024).

[15] F. Barato, Review of Alternative Sustainable Fuels for Hybrid Rocket Propulsion, Aerospace, 10(7), 643, (2023).

[16] J.A. Dallas, S. Raval, J.P. Alvarez Gaitan, S. Saydam, A.G. Dempster, The Environmental Impact of Emissions from Space Launches: A Comprehensive Review, Journal of Cleaner Production, 255, (2020).

[17] C. Paravan, A. Hashish, V. Santolini, Test Activities on Hybrid Rocket Engines: Combustion Analyses and Green Storable Oxidizers—A Short Review, Aerospace, 10(7), 572, (2023).

[18] I. Remissa, H. Jabri, Y. Hairch, K. Toshtay, M. Atamanov, S. Azat, R. Amrousse, Propulsion Systems, Propellants, Green Propulsion Subsystems and Their Applications: A Review, Eurasian Chemico-Technological Journal, 25(1), 3-19, (2023).

[19] X.-L. Liu, S.-Q. Hu, Y. Wang, W.-M. Zhang, L.-L. Liu, Droplet Entrainment Characteristics of HTPB/Paraffin Blended Fuels for Hybrid Rocket Motors, Acta Astronautica, 214, 293-302, (2024).

[20] F. D. A. Quadros, P. T. Lacava, Swirl Injection of Gaseous Oxygen in a Lab-Scale Paraffin Hybrid Rocket Motor, Journal of Propulsion and Power, 35(5), (2019).

[21] G.D. Di Martino, S. Mungiguerra, C. Carmicino, R. Savino, Computational Fluid-Dynamic Modeling of the Internal Ballistics of Paraffin-fueled Hybrid Rocket, Aerospace Science and Technology, 89, 431-444, (2019).

[22] H. Tian, X. Niu, X. Meng, X. Jiang, X. Gu, G. Cai, Numerical and Experimental Investigations of Micro Al Particle Additive on the Performances of HTPB Hybrid Rocket Motors, Acta Astronautica, 220, 449-461, (2024).

[23] S. Cassese, S. Mungiguerra, R. Guida, A. Cecere, R. Savino, Regression Rate and Performance Analysis via Ballistic Reconstruction of a Small-scale H2O2-based Hybrid Rocket Fuelled by Polyvinyl Chloride, Aerospace Science and Technology, 146, (2024).

[24] H. Tian, X. Jiang, H. Zhu, Z. Wang, G. Cai, Effect of Fuel Type on Spatial Distribution Characteristics for Nozzle Erosion in Hybrid Rocket Motors, Acta Astronautica, 222, 191-206, (2024).

[25] M. Bouziane, A.E.M. Bertoldi, P. Hendrick, M. Lefebvre, Experimental Investigation of the Axial Oxidizer Injectors Geometry on a 1-kN Paraffin-fueled Hybrid Rocket Motor, FirePhysChem, 1(4), 231-243, (2021).

[26] R. Wang, X. Lin, Z. Wang, K. Wu, J. Pan, Z. Zhang, J. Luo, F. Li, X. Yu, Effect of Characteristic Structure of Nested Composite Hybrid Rocket Fuel Grain on Combustion Properties, Acta Astronautica, 218, 269-281, (2024).

[27] Z. Zhang, X. Lin, Z. Wang, K. Wu, J. Luo, S. Fang, C. Zhang, F. Li, X. Yu, Effects of Swirl Injection on the Combustion of a Novel Composite Hybrid Rocket Fuel Grain, Acta Astronautica, 199, 174-182, (2022).

[28] C. Nguyen, J. C. Thomas, Performance of Additively Manufactured Fuels for Hybrid Rockets, Aerospace, 10(6), 500, (2023).

[29] M. Bouziane, A.E.M. Bertoldi, P. Milova, P. Hendrick, M. Lefebvre, Performance Comparison of Oxidizer Injectors in a 1-kN Paraffin-Fueled Hybrid Rocket Motor, Aerospace Science and Technology, 89, 392-406, (2019).

[30] A. Okninski, P. Surmacz, B. Bartkowiak,T. Mayer, K. Sobczak, M. Pakosz, D. Kaniewski, J. Matyszewski, G. Rarata, P. Wolanski, Development of Green Storable Hybrid Rocket Propulsion Technology Using 98% Hydrogen Peroxide as Oxidizer, Aerospace, 8(9), 234, (2021).

[31] W. Kopacz, A. Okninski, A. Kasztankiewicz, P. Nowakowski, G. Rarata, P. Maksimowski, Hydrogen Peroxide – A Promising Oxidizer for Rocket Propulsion and Its Application in Solid Rocket Propellants, FirePhysChem, 2(1), 56-66, (2022).

[32] G. Gallo, S. Mungiguerra, R. Savino, D. Cardillo, F. Battista, Effect of Grain Length on GOx-Paraffin Hybrid Rocket Engines Performance and Regression Rate, International Journal of Heat and Mass Transfer, 220, (2024).

[33] Y. Wu, Z. Zhang, Q. Wang, N. Wang, Combustion Characteristics of Skeleton Polymer Reinforced Paraffin-wax Fuel Grain for Applications in Hybrid Rocket Motors, Combustion and Flame, 241, (2022).

[34] J. C. Thomas, C. Paravan, J. M. Stahl, A. J. Tykol, F. A. Rodriguez, L. Galfetti, E. L. Petersen, Experimental Evaluation of HTPB/Paraffin Fuel Blends for Hybrid Rocket Applications, Combustion and Flame, 229, (2021).

[35] C. Oztan, E. Ginzburg, M. Akin, Y. Zhou, R. M. Leblanc, V. Coverstone, 3D Printed ABS/Paraffin Hybrid Rocket Fuels with Carbon Dots for Superior Combustion Performance, Combustion and Flame, 225, 428-434, (2021).

[36] L.-L. Liu, X. He, Y. Wang, Z.-B Chen, Q. Guo, Regression Rate of Paraffin-based Fuels in Hybrid Rocket Motor, Aerospace Science and Technology, 107, (2020).

[37] M. T. Migliorino, M. Fabiani, C. Paravan, D. Bianchi, F. Nasuti, L. Galfetti, R. C. Pellegrini, E. Cavallini, Numerical and Experimental Analysis of Fuel Regression Rate in a Lab-scale Hybrid Rocket Engine with Swirl Injection, Aerospace Science and Technology, 140, (2023).

[38] N. A. B. M. Jamil, A. H. B. Mohamaddiah, M. H. B. Azami, N. H. Nordin, High Entropy Alloy as Metal Additive for Hybrid Rocket Propellant, Materialstoday:Proceedings, 75(1), 140-146, (2023).

[39] Y. Pal, S. K. Palateerdham, S. N. Mahottamananda, S. Sivakumar, A. Ingenito, Combustion Performance of Hybrid Rocket Fuels Loaded with MgB2 and Carbon Black Additives, Propulsion and Power Research, 12(2), 212-226, (2023).

DEPARTMENT OF ASTRONAUTICAL ENGINEERING, FACULTY OF AERONAUTICS AND ASTRONAUTICS, KAYSERİ, TÜRKİYE
E-mail address: sureyyavarol@erciyes.edu.tr

DEPARTMENT OF ASTRONAUTICAL ENGINEERING, FACULTY OF AERONAUTICS AND ASTRONAUTICS, KAYSERİ, TÜRKİYE
E-mail address: balbayrak@erciyes.edu.tr

DEPARTMENT OF ASTRONAUTICAL ENGINEERING, FACULTY OF AERONAUTICS AND ASTRONAUTICS, KAYSERİ, TÜRKİYE
E-mail address: nafiz@erciyes.edu.tr

IFSCOM-E 2024
10th Ifs And Contemporary Mathematics and Engineering Conference
04-07 September 2024, Mersin, Türkiye
ISBN:978-625-97923-1-6
pp:97-102

HYPER-DUAL NUMBERS RELATED TO GENERALIZED TRIBONACCI NUMBERS

TÜLAY YAĞMUR

0000-0002-6224-1921

Abstract. The objective of this study is to introduce a new class of hyper-dual numbers. These numbers are formed by taking the generalized Tribonacci numbers as coefficients instead of real numbers in hyper-dual numbers. Then, some of their properties such as the recurrence relation, Binet's formula, ordinary generating function, exponential generating function, and Poisson generating function are presented.

1. Introduction

Dual numbers, which are an extension of real numbers, were introduced by Clifford [1]. The form of a dual number x is

$$x = a + b\varepsilon,$$

where a, b are real numbers and ε is the dual unit such that $\varepsilon^2 = 0$, $\varepsilon \neq 0$.

Hyper-dual numbers, which are an extension of dual numbers, were introduced by Fike and Alonso [2, 3]. A hyper-dual number z has the form

$$z = x_1 + x_2\varepsilon^*,$$

where x_1, x_2 are dual numbers and ε^* is the dual unit. Moreover, a hyper-dual number z can be written as

$$z = a_0 + a_1\varepsilon + a_2\varepsilon^* + a_3\varepsilon\varepsilon^*,$$

where a_0, a_1, a_2, a_3 are real numbers and ε, ε^* are the dual units that satisfy the rules

$$\varepsilon^2 = {\varepsilon^*}^2 = (\varepsilon\varepsilon^*)^2 = 0, \quad \varepsilon \neq \varepsilon^*, \quad \varepsilon\varepsilon^* = \varepsilon^*\varepsilon, \quad \varepsilon, \varepsilon^*, \varepsilon\varepsilon^* \neq 0. \tag{1.1}$$

Date: September, 20, 2024.
2000 *Mathematics Subject Classification.* 11B37, 11B39, 11B83, 11R52.
Key words and phrases. Hyper-Dual number, Generalized Tribonacci number, Third-Order recurrence relation

.

Let $z_1 = a_0+a_1\varepsilon+a_2\varepsilon^*+a_3\varepsilon\varepsilon^*$ and $z_2 = b_0+b_1\varepsilon+b_2\varepsilon^*+b_3\varepsilon\varepsilon^*$ be two hyper-dual numbers. Then, the addition and multiplication of hyper-dual numbers are given as

$$z_1 + z_2 = (a_0 + b_0) + (a_1 + b_1)\varepsilon + (a_2 + b_2)\varepsilon^* + (a_3 + b_3)\varepsilon\varepsilon^*$$

and

$$z_1 z_2 = a_0b_0 + (a_0b_1 + a_1b_0)\varepsilon + (a_0b_2 + a_2b_0)\varepsilon^* + (a_0b_3 + a_1b_2 + a_2b_1 + a_3b_0)\varepsilon\varepsilon^*,$$

respectively. For detailed information about hyper-dual numbers, we refer to [3].

In recent years, many authors have studied hyper-dual numbers whose coefficients taken from special integer sequences' elements. For example, in [4], Ömür and Koparal introduced the hyper-dual generalized Fibonacci and Lucas numbers, and gave some properties for these numbers. Then, in [5], Ait-Amrane et al. defined the hyper-dual Horadam numbers, and introduced a new class of quaternions with the hyper-dual Horadam number components. Moreover, in [6], Karakuş et al. studied the hyper-dual Leonardo numbers.

In this study, we will consider the generalized Tribonacci sequence.The generalized Tribonacci sequence $\{V_n(V_0, V_1, V_2; p, q, r)\}_{n\geq 0}$, in short $\{V_n\}_{n\geq 0}$, is defined recursively by the relation

$$V_n = pV_{n-1} + qV_{n-2} + rV_{n-3}, \quad n \geq 3 \tag{1.2}$$

with the initial conditions $V_0 = a$, $V_1 = b$, $V_2 = c$. Here, a, b, c are arbitrary integers and p, q, r are real numbers.

The characteristic equation of the third-order recurrence relation in Eq.(1.2) is $t^3-pt^2-qt-r = 0$. Let α, β and γ are the roots of the equation $t^3-pt^2-qt-r = 0$. The direct formula, i.e., Binet's formula for the nth generalized Tribonacci number is given by

$$V_n = \frac{P\alpha^n}{(\alpha-\beta)(\alpha-\gamma)} + \frac{Q\beta^n}{(\beta-\alpha)(\beta-\gamma)} + \frac{R\gamma^n}{(\gamma-\alpha)(\gamma-\beta)}, \tag{1.3}$$

where

$$\begin{aligned} P &:= c - (\beta+\gamma)b + \beta\gamma a, \\ Q &:= c - (\alpha+\gamma)b + \alpha\gamma a, \\ R &:= c - (\alpha+\beta)b + \alpha\beta a. \end{aligned}$$

Several authors have examined the generalized Tribonacci sequence, see, for instance, [7, 8, 9, 10]. It is easy to see that many third-order linear recurrence sequences such as Tribonacci sequence [11], Narayana sequence [12], Perrin sequence [13] can be deduced as particular cases of the generalized Tribonacci sequence by taking appropriate values for a, b, c, p, q, r.

Motivated by the previously mentioned studies, our goal in this study is to define and study hyper-dual numbers with the generalized Tribonacci number components.

2. Main results

In this section, we first give the definition of hyper-dual numbers with the generalized Tribonacci number components. Then, we investigate some basic properties of these numbers.

Definition 2.1. For non-negative integer n, the nth hyper-dual number whose coefficients from the generalized Tribonacci numbers is defined as

$$HDV_n = V_n + V_{n+1}\varepsilon + V_{n+2}\varepsilon^* + V_{n+3}\varepsilon\varepsilon^*, \tag{2.1}$$

where V_n is the nth generalized Tribonacci number and ε, ε^* are the dual units that satisfy the rules in Eq.(1.1).

The first three hyper-dual numbers with the generalized Tribonacci number components are as the following:

$$\begin{aligned}
HDV_0 &= a + b\varepsilon + c\varepsilon^* + (pc + qb + ra)\varepsilon\varepsilon^*,\\
HDV_1 &= b + c\varepsilon + (pc + qb + ra)\varepsilon^* + ((p^2+q)c + (pq+r)b + pra)\varepsilon\varepsilon^*,\\
HDV_2 &= c + (pc + qb + ra)\varepsilon + ((p^2+q)c + (pq+r)b + pra)\varepsilon^*\\
&\quad +((p^3+2pq+r)c + (p^2q+q^2+pr)b + (p^2r+qr)a)\varepsilon\varepsilon^*.
\end{aligned}$$

Let HDV_n and HDV_m be the nth and mth hyper-dual numbers whose coefficients from the generalized Tribonacci numbers. Then, the addition and multiplication of HDV_n and HDV_m are given as

$$\begin{aligned}
HDV_n + HDV_m &= (V_n + V_m) + (V_{n+1} + V_{m+1})\varepsilon + (V_{n+2} + V_{m+2})\varepsilon^*\\
&\quad +(V_{n+3} + V_{m+3})\varepsilon\varepsilon^*
\end{aligned}$$

and

$$\begin{aligned}
HDV_nHDV_m &= V_nV_m + (V_nV_{m+1} + V_{n+1}V_m)\varepsilon + (V_nV_{m+2} + V_{n+2}V_m)\varepsilon^*\\
&\quad +(V_nV_{m+3} + V_{n+1}V_{m+2} + V_{n+2}V_{m+1} + V_{n+3}V_m)\varepsilon\varepsilon^*,
\end{aligned}$$

respectively.

Theorem 2.2. *For $n \geq 3$, the recurrence relation of the hyper-dual numbers with the generalized Tribonacci number components is*

$$HDV_n = pHDV_{n-1} + qHDV_{n-2} + rHDV_{n-3}. \tag{2.2}$$

Proof. From Eq.(1.2) and Eq.(2.1), we have

$$\begin{aligned}
pHDV_{n-1} + qHDV_{n-2} + rHDV_{n-3} &= p(V_{n-1} + V_n\varepsilon + V_{n+1}\varepsilon^* + V_{n+2}\varepsilon\varepsilon^*)\\
&\quad +q(V_{n-2} + V_{n-1}\varepsilon + V_n\varepsilon^* + V_{n+1}\varepsilon\varepsilon^*)\\
&\quad +r(V_{n-3} + V_{n-2}\varepsilon + V_{n-1}\varepsilon^* + V_n\varepsilon\varepsilon^*)\\
&= (pV_{n-1} + qV_{n-2} + rV_{n-3})\\
&\quad +(pV_n + qV_{n-1} + rV_{n-2})\varepsilon\\
&\quad +(pV_{n+1} + qV_n + rV_{n-1})\varepsilon^*\\
&\quad +(pV_{n+2} + qV_{n+1} + rV_n)\varepsilon\varepsilon^*\\
&= V_n + V_{n+1}\varepsilon + V_{n+2}\varepsilon^* + V_{n+3}\varepsilon\varepsilon^*\\
&= HDV_n.
\end{aligned}$$

□

Theorem 2.3. *For non-negative integer n, the following relations hold:*

$$\begin{aligned} HDV_n - HDV_{n+1}\varepsilon - HDV_{n+2}\varepsilon^* - HDV_{n+3}\varepsilon\varepsilon^* &= V_n - 2V_{n+3}\varepsilon\varepsilon^*, \\ HDV_n - HDV_{n+1}\varepsilon + HDV_{n+2}\varepsilon^* - HDV_{n+3}\varepsilon\varepsilon^* &= V_n + 2V_{n+2}\varepsilon^*. \end{aligned}$$

Proof. By using Eq.(2.1) and the multiplication rules in Eq.(1.1), we can obtain the results. □

Theorem 2.4. *For $n \geq 0$, Binet's formula of the nth number HDV_n is*

$$V_n = \frac{P\bar{\alpha}\alpha^n}{(\alpha-\beta)(\alpha-\gamma)} + \frac{Q\bar{\beta}\beta^n}{(\beta-\alpha)(\beta-\gamma)} + \frac{R\bar{\gamma}\gamma^n}{(\gamma-\alpha)(\gamma-\beta)}, \tag{2.3}$$

where P, Q, R are defined as in Eq.(1.3) and

$$\begin{aligned} \bar{\alpha} &:= 1 + \alpha\varepsilon + \alpha^2\varepsilon^* + \alpha^3\varepsilon\varepsilon^*, \\ \bar{\beta} &:= 1 + \beta\varepsilon + \beta^2\varepsilon^* + \beta^3\varepsilon\varepsilon^*, \\ \bar{\gamma} &:= 1 + \gamma\varepsilon + \gamma^2\varepsilon^* + \gamma^3\varepsilon\varepsilon^*. \end{aligned}$$

Proof. By virtue of Eq.(2.1) and Binet's formula for the generalized Tribonacci numbers given in Eq.(1.3), we get

$$\begin{aligned} HDV_n &= V_n + V_{n+1}\varepsilon + V_{n+2}\varepsilon^* + V_{n+3}\varepsilon\varepsilon^* \\ &= \left(\frac{P\alpha^n}{(\alpha-\beta)(\alpha-\gamma)} + \frac{Q\beta^n}{(\beta-\alpha)(\beta-\gamma)} + \frac{R\gamma^n}{(\gamma-\alpha)(\gamma-\beta)}\right) \\ &\quad + \left(\frac{P\alpha^{n+1}}{(\alpha-\beta)(\alpha-\gamma)} + \frac{Q\beta^{n+1}}{(\beta-\alpha)(\beta-\gamma)} + \frac{R\gamma^{n+1}}{(\gamma-\alpha)(\gamma-\beta)}\right)\varepsilon \\ &\quad + \left(\frac{P\alpha^{n+2}}{(\alpha-\beta)(\alpha-\gamma)} + \frac{Q\beta^{n+2}}{(\beta-\alpha)(\beta-\gamma)} + \frac{R\gamma^{n+2}}{(\gamma-\alpha)(\gamma-\beta)}\right)\varepsilon^* \\ &\quad + \left(\frac{P\alpha^{n+3}}{(\alpha-\beta)(\alpha-\gamma)} + \frac{Q\beta^{n+3}}{(\beta-\alpha)(\beta-\gamma)} + \frac{R\gamma^{n+3}}{(\gamma-\alpha)(\gamma-\beta)}\right)\varepsilon\varepsilon^* \\ &= \frac{P\alpha^n(1+\alpha\varepsilon+\alpha^2\varepsilon^*+\alpha^3\varepsilon\varepsilon^*)}{(\alpha-\beta)(\alpha-\gamma)} \\ &\quad + \frac{Q\beta^n(1+\beta\varepsilon+\beta^2\varepsilon^*+\beta^3\varepsilon\varepsilon^*)}{(\beta-\alpha)(\beta-\gamma)} \\ &\quad + \frac{R\gamma^n(1+\gamma\varepsilon+\gamma^2\varepsilon^*+\gamma^3\varepsilon\varepsilon^*)}{(\gamma-\alpha)(\gamma-\beta)} \\ &= \frac{P\bar{\alpha}\alpha^n}{(\alpha-\beta)(\alpha-\gamma)} + \frac{Q\bar{\beta}\beta^n}{(\beta-\alpha)(\beta-\gamma)} + \frac{R\bar{\gamma}\gamma^n}{(\gamma-\alpha)(\gamma-\beta)}. \end{aligned}$$

Thus, we get the desired result. □

Theorem 2.5. *The ordinary generating function for the hyper-dual numbers with the generalized Tribonacci number components is*

$$G(t) = \frac{HDV_0 + (HDV_1 - pHDV_0)t + (HDV_2 - pHDV_1 - qHDV_0)t^2}{1 - pt - qt^2 - rt^3}.$$

Proof. According to the general theory of the ordinary generating function for the sequence, we can write

$$G(t) = \sum_{n=0}^{\infty} HDV_n t^n.$$

Then, considering Eq.(2.2), we have

$$\begin{aligned}
G(t) &= HDV_0 + HDV_1 t + HDV_2 t^2 + \sum_{n=3}^{\infty} HDV_n t^n \\
&= HDV_0 + HDV_1 t + HDV_2 t^2 + \sum_{n=3}^{\infty} (pHDV_{n-1} + qHDV_{n-2} + rHDV_{n-3}) t^n \\
&= HDV_0 + HDV_1 t + HDV_2 t^2 + pt \sum_{n=3}^{\infty} HDV_{n-1} t^{n-1} + qt^2 \sum_{n=3}^{\infty} HDV_{n-2} t^{n-2} \\
&\quad + rt^3 \sum_{n=3}^{\infty} HDV_{n-3} t^{n-3} \\
&= HDV_0 + HDV_1 t + HDV_2 t^2 - pt(HDV_0 + HDV_1 t) + pt \sum_{n=0}^{\infty} HDV_n t^n \\
&\quad - qt^2 HDV_0 + qt^2 \sum_{n=0}^{\infty} HDV_n t^n + rt^3 \sum_{n=0}^{\infty} HDV_n t^n \\
&= HDV_0 + (HDV_1 - pHDV_0)t + (HDV_2 - pHDV_1 - qHDV_0)t^2 \\
&\quad + ptG(t) + qt^2 G(t) + rt^3 G(t).
\end{aligned}$$

Then, it follows that

$$(1 - pt - qt^2 - rt^3)G(t) = HDV_0 + (HDV_1 - pHDV_0)t + (HDV_2 - pHDV_1 - qHDV_0)t^2$$

which is the desired result. □

Theorem 2.6. *The exponential generating function for the hyper-dual numbers with the generalized Tribonacci number components is*

$$EG(t) = \frac{P\bar{\alpha}}{(\alpha-\beta)(\alpha-\gamma)} e^{\alpha t} + \frac{Q\bar{\beta}}{(\beta-\alpha)(\beta-\gamma)} e^{\beta t} + \frac{R\bar{\gamma}}{(\gamma-\alpha)(\gamma-\beta)} e^{\gamma t}.$$

Proof. Via Eq.(2.3), we have

$$\begin{aligned}
EG(t) &= \sum_{n=0}^{\infty} HDV_n \frac{t^n}{n!} \\
&= \sum_{n=0}^{\infty} \left(\frac{P\bar{\alpha}\alpha^n}{(\alpha-\beta)(\alpha-\gamma)} + \frac{Q\bar{\beta}\beta^n}{(\beta-\alpha)(\beta-\gamma)} + \frac{R\bar{\gamma}\gamma^n}{(\gamma-\alpha)(\gamma-\beta)} \right) \frac{t^n}{n!} \\
&= \frac{P\bar{\alpha}}{(\alpha-\beta)(\alpha-\gamma)} \sum_{n=0}^{\infty} \frac{(\alpha t)^n}{n!} + \frac{Q\bar{\beta}}{(\beta-\alpha)(\beta-\gamma)} \sum_{n=0}^{\infty} \frac{(\beta t)^n}{n!} \\
&\quad + \frac{R\bar{\gamma}}{(\gamma-\alpha)(\gamma-\beta)} \sum_{n=0}^{\infty} \frac{(\gamma t)^n}{n!} \\
&= \frac{P\bar{\alpha}}{(\alpha-\beta)(\alpha-\gamma)} e^{\alpha t} + \frac{Q\bar{\beta}}{(\beta-\alpha)(\beta-\gamma)} e^{\beta t} + \frac{R\bar{\gamma}}{(\gamma-\alpha)(\gamma-\beta)} e^{\gamma t}.
\end{aligned}$$

Hence, the desired result is obtained. □

As a consequence of Theorem 2.6, the Poisson generating function for the hyper-dual numbers with the generalized Tribonacci number components is given in the following result.

Corollary 2.7. *The Poisson generating function for the hyper-dual numbers with the generalized Tribonacci number components is*

$$\begin{aligned} PG(t) &= \sum_{n=0}^{\infty} HDV_n \frac{t^n}{n!} e^{-t} \\ &= \frac{P\bar{\alpha}}{(\alpha-\beta)(\alpha-\gamma)} e^{(\alpha-1)t} + \frac{Q\bar{\beta}}{(\beta-\alpha)(\beta-\gamma)} e^{(\beta-1)t} + \frac{R\bar{\gamma}}{(\gamma-\alpha)(\gamma-\beta)} e^{(\gamma-1)t}. \end{aligned}$$

3. Conclusions

The present study examines hyper-dual numbers whose coefficients from the generalized Tribonacci numbers. In this study, the recurrence relation, Binet's formula and generating functions of these numbers were obtained.

References

[1] W.K. Clifford, Preliminary Sketch of Biquaternions, Proceedings of the London Mathematical Society, s1-4(1), 381-395, (1873).
[2] J.A. Fike, Numerically Exact Derivate Calculations Using Hyper-Dual Numbers, In: 3rd Annual Student Joint Workshop in Simulation-Based Engineering and Design, (2009).
[3] J.A. Fike, J.J. Alonso, The Development of Hyper-Dual Numbers for Exact Second-Derivate Calculations, In: 49th AIAA Aerospace Sciences Meeting Including the New Horizons Forum and Aerospace Exposition, Orlando, Florida,(2011).
[4] N. Ömür, S. Koparal, On Hyper-Dual Generalized Fibonacci Numbers, Notes on Number Theory and Discrete Mathematics 26(1), 191-198, (2020).
[5] N.R. Ait-Amrane, İ. Gök, E. Tan, Hyper-Dual Horadam Quaternions, Miskolc Mathematical Notes, 22(2), 903-913, (2021).
[6] S.Ö. Karakuş, S.K. Nurkan, M. Turan, Hyper-Dual Leonardo Numbers, Konuralp Journal of Mathematics, 10(2), 269-275, (2022).
[7] A.G. Shannon, A.F. Horadam, Some Properties of Third-Order Recurrence Relations, The Fibonacci Quarterly, 10(2), 135-145, (1972).
[8] C.C. Yalavigi, Properties of Tribonacci Numbers, The Fibonacci Quarterly, 10(3), 231-246, (1972).
[9] S. Pethe, Some Identities for Tribonacci Sequences, The Fibonacci Quarterly, 26(2), 144-151, (1988).
[10] G. Cerda-Morales, On a Generalization for Tribonacci Quaternions, Mediterranean Journal of Mathematics, 14(6), Article:239, (2017).
[11] M. Feinberg, Fibonacci-Tribonacci, The Fibonacci Quarterly, 1(3), 71-74, (1963).
[12] J.P. Allouche, T. Johnson, Narayana's Cows and Delayed Morphisms, In: Articles of 3rd Computer Music Conference JIM96, France, (1996).
[13] A.G. Shannon, P.G. Anderson, A.F. Horadam, Properties of Cordonnier, Perrin and Van der Laan Numbers, International Journal of Mathematical Education in Science and Technology, 37(7), 825-831, (2006).

Department of Mathematics, Aksaray University, 68100 Aksaray, Türkiye
Email address: tulayyagmur@aksaray.edu.tr

IFSCOM-E 2024
10th Ifs And Contemporary Mathematics and Engineering Conference
04-07 September 2024, Mersin, Türkiye
ISBN:978-625-97923-1-6
pp:103-108

SIMILARITY METRIC AND ITS RELATIONS BETWEEN OTHER METRICS

MEHMET SOLGUN, KEMAL TAŞKÖPRÜ, AND ESRA GÜDER

0000-0002-2275-7763, 0000-0002-0760-3782 and 0009-0005-0422-863X

Abstract. In this paper, we focus on the notion of similarity metric spaces, partial metric spaces and (weighted) quasi metric spaces with their certain properties. Furthermore, we investigate the relations of these structures on a given set and give various examples.

1. Introduction

As one of the most common ways of comparing objects is the measure of distance, interpreting and measuring the similarity of objects is also conventionally associated with distance. Similarity, as expressed by [1], could not be only based on distance, but also on the amount of common features. Although the concept of similarity is used in various fields such as physics, statistics, data science, psychology, etc., (see [1–7]) the formal axiomatic definition of similarity metric that we consider is first defined in [8]. By using this definition, the duality of similarity and distance is recently studied by [9]. Also, the partial and (weighted) quasi metric is used to examine partially defined data that is likely to occur in computer science and is defined as an extension of the distance metric, where the self-distance may not always be zero [10,11]. A considerable number of studies about quasi metric spaces and partial metric spaces exist which are relevant to the topological properties of them, the fixed point theory and theoretic computer science (See [12–20] and others in them). In this study, we focus on the relations of similarity metric with quasi metric and partial metric functions on a given set U and give elegant ways to construct a similarity metric from a quasi metric and partial metric on a non-empty set U, and state the correspondence between these structures and a similarity metric. Also, we present coherent examples about the idea.

2. The Similarity Spaces

Definition 2.1. Let $U \neq \emptyset$ and $s : U \times U \to \mathbb{R}$ be a function satisfying the axioms

Date: September, 20, 2024.
2010 *Mathematics Subject Classification.* 54A05; 54E35.
Key words and phrases. Similarity, Similarity metric, Quasi metric, Partial metric.

S1. $s(v,v) \geq 0$,
S2. $s(v,v) \geq s(v,w)$,
S3. $s(v,w) = s(w,v)$,
S4. $s(v,v) = s(v,w) = s(w,w) \Leftrightarrow v = w$,
S5. $s(v,z) \geq s(v,w) + s(w,z) - s(w,w)$

for all $v, w, z \in U$. Then, the function s is said to be a similarity metric on U and (U,s) is called a similarity space. Also, s is said to be normalized similarity metric if $|s(v,w)| \leq 1$ for every $v, w \in U$ [8].

As it is seen, with a similarity function, one can analogize the similarities of objects of a set. Contrary to distance measures, as two objects v, w get "similar" to each other, the value $s(v,w)$ gets bigger.

Example 2.2. The well known Jaccard index in statistics measures the similarity between finite sets of samples V and W from a population X and is denoted by

$$J(V,W) = \frac{|V \cap W|}{|V \cup W|}.$$

This is a simple similarity metric on X and so (X,J) is a similarity space. These and similar examples can be found in [8, 9].

Also, in the studies [1,8], similarity and distance are considered interchangeably. By way of example, let (U,d) be a metric space and consider the function $s(v,w) = d(v,\tilde{v}) + d(w,\tilde{v}) - d(v,w)$ for a fixed element $\tilde{v} \in U$ and all $v, w \in U$. It can be seen that s satisfies *S1-S5* and so (U,s) is a similarity space.

3. The relations between similarity metric and other metric structures

The correspondence between a distance metric, a partial metric and a quasi metric has been studied by many authors. This section is reserved for the basic notions and definitions about the quasi metric and the partial metric. Then, we evaluate the relations of these structures with a (given) similarity metric.

Definition 3.1. Let $U \neq \emptyset$ and $q : U \times U \to \mathbb{R}$ be a function satisfying the following axioms for all $v, w, z \in U$.

Q1. $q(v,w) \geq 0$,
Q2. $q(v,w) = q(w,v) = 0 \Leftrightarrow v = w$,
Q3. $q(v,z) \leq q(v,w) + q(w,z)$.

Then, the function q is called a quasi metric on U and (U,q) is said to be a quasi metric space. It is well known that the quasi metric is an asymmetric distance function. The conjugate (quasi metric) of q is defined by $q^*(v,w) = q(w,v)$ for every $v, w \in U$ which is also a quasi metric. Moreover, a quasi metric space (U,q) is called "weighted" and denoted by (U,q,φ) if there exists a function $\varphi : U \to \mathbb{R}$ with

$$\varphi(v) + q(v,w) = \varphi(w) + q(w,v). \tag{3.1}$$

In particular case, if $\varphi(U) \subset [0,\infty)$, then the space is called positively weighted. For detailed information, see [21–24] and others in them.

Example 3.2. Let $q : \mathbb{R}^2 \to \mathbb{R}_0^+$ be given by

$$q(v,w) = max\{w - v, 0\},$$

for all $v, w \in \mathbb{R}$. Then, it can be seen that the function q satisfies $Q1 - Q3$. So, q is a quasi metric function. Moreover, The space can be considered as weighted with the function $\varphi : \mathbb{R} \to \mathbb{R}$, with $\varphi(v) = v$.

Example 3.3. Let $q(K, L)$ be defined as the cost of the travel from the departure city K to the arrival city L. Then, obviously $q(K, L) \geq 0$ and $q(K, L) = 0$ if and only if $K = L$. Also, one can consider that $q(K, M) \leq q(K, L) + q(L, M)$ for all cities K, L, M. On the other hand, depending on the supply-demand and taxes, the prices $q(K, L)$ and $q(L, K)$ could be slightly different. In this manner, the function q is a quasi metric function. Also, by considering $\varphi(K)$ to be the local tax for leaving the city K with

$$q(K, L) + \varphi(K) = q(L, K) + \varphi(L),$$

for any cities K, L, we get the positively (weighted) quasi metric space (U, q, φ), on the set of the cities U [24].

Definition 3.4. Let $U \neq \emptyset$ and $p : U \times U \to \mathbb{R}$ be a function with the followings for all $v, w, z \in U$.

P1. $p(v, w) \geq p(v, v) \geq 0$,
P2. $p(v, w) = p(w, v)$,
P3. $p(v, v) = p(v, w) = p(w, w) \Leftrightarrow v = w$,
P4. $p(v, z) \leq p(v, w) + p(w, z) - p(w, w)$.

Then, the function p is called a partial metric on U and (U, p) is said to be a partial metric space.

Obviously, any metric space is a partial metric space. Another partial metric example is as follows:

Example 3.5. Let U be the collection of all closed intervals, $[v, w] \subset \mathbb{R}$, and $p : U^2 \to [0, \infty)$ be defined as

$$p([v, w], [z, t]) = max\{w, t\} - min\{v, z\}.$$

Then, p is a partial metric on U.

Example 3.6. Let $U = \mathbb{R}$ and the function p be as, $p(\alpha, \beta) = e^{max\{\alpha,\beta\}}$ for all $\alpha, \beta \in U$. Then, by direct calculation, in can be seen that (U, p) is a partial metric space.

In [11], it is shown that one can obtain a (weighted) quasi metric from a partial metric and vice versa. For detailed information, see [10, 11].

Now, we give the relations between these structures and similarity metric on a given set U.

Proposition 1. Let (U, s) be a similarity space and define $q_s : U \times U \to \mathbb{R}$ as

$$q_s(v, w) = s(v, v) - s(v, w)$$

for all $v, w \in U$. Then, (U, q_s) is a quasi metric space.

Proof. The mapping q_s satisfies the axioms *Q1-Q3* as follows:

Q1. It follows from the axiom *S2*.
Q2. If $q_s(v, w) = q_s(w, v) = 0$ for all $v, w \in U$, then $q_s(v, w) = s(v, v) - s(v, w) = 0$ and $q_s(w, v) = s(w, w) - s(w, v) = 0$. So, we have $s(v, v) = s(v, w) = s(w, w)$ from the axiom *S3* and hence $v = w$ from the axiom *S4*. Also, the converse is obvious.

Q3. For all $v, w, z \in U$, the result is obtained by using the axiom *S5* as follows:

$$\begin{aligned} q_s(v,z) &= s(v,v) - s(v,z) \\ &\leq s(v,v) - [s(v,w) + s(w,z) - s(w,w)] \\ &= s(v,v) - s(v,w) + s(w,w) - s(w,z) \\ &= q_s(v,w) + q_s(w,z). \end{aligned}$$

Thus, q_s is a quasi metric. □

Remark 3.7. In particular, if there exists $M \in \mathbb{R}$ such that, $s(v,w) < M$ for any $v, w \in U$, then the function $\varphi_s(v) := M - s(v,u)$ is indeed a weight function for (U, q_s). Thus, one can obtain a (weighted) quasi metric from a given s, under the condition of the existence such M. As a corollary, a (weighted) quasi metric can be obtained from a normalized similarity metric.

On the contrary to the above proposition, one may not be able to obtain a similarity metric from a quasi metric. To do that, we also need a weight function on (U, q).

Proposition 2. Let (U, q, φ_q) be a (weighted) quasi metric space and $s_q : U \times U \to \mathbb{R}$ be a function as

$$s_q(v,w) = \varphi_q(v) - q(w,v)$$

for all $v, w \in U$. Then, (U, s_q) is a similarity metric space.

Proof. The mapping s_q satisfies the axioms *S1-S5* as follows:

S1. It follows from the axiom *Q2* and the definition of φ.

S2. For all $v, w \in U$, we get the result by using the axioms *Q1* and *Q2* as below:

$$s_q(v,v) - s_q(v,w) = \varphi_q(v) - q(v,v) - \varphi_q(v) + q(w,v) \geq 0.$$

S3. For all $v, w \in U$, we get the result by using the condition (3.1) as below:

$$\begin{aligned} s_q(v,w) - s_q(w,v) &= \varphi_q(v) - q(w,v) - \varphi_q(w) + q(v,w) \\ &= \varphi_q(v) - \varphi_q(w) - q(w,v) + q(v,w) \\ &= q(w,v) - q(v,w) - q(w,v) + q(v,w) \\ &= 0. \end{aligned}$$

S4. For all $v, w \in U$, if $s_q(v,v) = s_q(v,w)$, then we have $\varphi_q(v) = \varphi_q(v) - q(w,v)$ and hence $q(w,v) = 0$. Similarly, if $s_q(w,w) = s_q(v,w)$ and we use the axiom *S3*, then we have $\varphi_q(w) = \varphi_q(w) - q(v,w)$ and hence $q(v,w) = 0$. Thus, we obtain $v = w$ from the axiom *Q2*. Also, the converse is obvious.

S5. For all $v, w, z \in U$, we obtain the result by using the axioms *Q2* and *Q3* as below:

$$\begin{aligned} s_q(v,z) &= \varphi_q(v) - q(z,v) \\ &\geq \varphi_q(v) - [q(z,w) + q(w,v)] \\ &= \varphi_q(v) - q(w,v) + \varphi_q(w) - q(z,w) - \varphi_q(w) - q(w,w) \\ &= s_q(v,w) + s_q(w,z) - s_q(w,w). \end{aligned}$$

Thus, s_q is a similarity metric. □

Remark 3.8. Note that, with keeping the notation above in mind, by constructing the quasi metric q_{s_q} that is deduced from the similarity metric s_q, we indeed obtained q^*, the conjugate of q. In a word, $q_{s_q} = q^*$. In addition, if there exists M with $s_q(v, w) < M$ for all $v, w \in U$, $\varphi_{q_{s_q}} = M - \varphi_q$.

For a given similarity metric s on U, it is proven that the function $d(v, w) = s(v, v) + s(w, w) - 2s(v, w)$ is a distance metric [9]. So, we can state the following corollary:

Corollary 3.9. Let (U, s) be a similarity space. Then, the function $d_s = q_s + q_s^*$ obtained as

$$d_s(v, w) = s(v, v) + s(w, w) - 2s(v, w)$$

is a distance metric.

We can state the following two propositions by considering the correspondence of the partial metrics and the (weighted) quasi metrics, studied by [11].

Proposition 3. Let (U, p) be a partial metric space and $s_p : U \times U \to \mathbb{R}$ be a function such that

$$s_p(v, w) = p(v, v) + p(w, w) - p(v, w)$$

for all $v, w \in U$. Then, (U, s_p) is a similarity metric space.

Proof. From [11], (U, q, φ) is a (weighted) quasi metric space with $q(v, w) = p(v, w) - p(v, v)$ and $\varphi(v) = p(v, v)$. Then, from Proposition 2, we have a similarity metric $s(v, w) = \varphi(v) - q(w, v)$. Hence, $s(v, w) = p(v, v) - p(v, w) + p(w, w)$. □

Example 3.10. Let $(\mathbb{R}^+, p)$ be partial metric space with $p(v, w) = \max\{v, w\}$. Then, from Proposition 3, one can see that $s(v, w) = v + w - \max\{v, w\}$ is a similarity metric on $\mathbb{R}^+$.

Proposition 4. Let (U, s) be a similarity metric space with $M \in \mathbb{R}$ with $s(v, w) < M$, and $p_s : U \times U \to \mathbb{R}$ be a function such that

$$p_s(v, w) = M - s(v, w)$$

for every $v, w \in U$. Then, (U, p_s) is a partial metric space.

Proof. As we mentioned before, (U, q_s, φ) is a (weighted) quasi metric with $q_s(v, w) = s(v, v) - s(v, w)$ and $\varphi(v) = M - s(v, v)$. Then, the partial metric p corresponding to q_s is $p(v, w) = \varphi(v) + q_s(v, w)$. Hence, $p(v, w) = M - s(v, w)$. □

References

[1] C. H. Elzinga, Distance, Similarity and Sequence Comparison, Advances in Sequence Analysis: Theory, Method, Applications, 1.4, 51-73, (2014).

[2] S. A. Bero, A. K. Muda, Y. H. Choo, N. A. Muda, S. F. Pratama, Similarity measure for molecular structure: A brief review, J. Phys.: Conf. Ser., 892(012015): 1-8, (2017).

[3] C. H. Elzinga, M. Studer, Normalization of Distance and Similarity in Sequence Analysis, Sociol. Methods Res., 48(4), 877-904, (2019).

[4] R. Heckmann, Similarity, topology, and uniformity, J. Log. Algebr. Program., 79(1), 10-31, (2010).

[5] R. Rousseau, Jaccard similarity leads to the Marczewski-Steinhaus topology for information retrieval, Inf. Process. Manag., 34(1), 87-94, (1998).

[6] A. Tversky, Features of similarity, Psychol. Rev., 84(4), 327-352, (1977).

[7] S. T. Wierzchoń, M. A. Kłopotek, Cluster Analysis, Modern Algorithms of Cluster Analysis, 2, 9-66, (2018).

[8] S. Chen, B. Ma, K. Zhang, On the similarity metric and the distance metric, Theor. Comput. Sci., 410(24–25), 2365-2376, (2009).
[9] O. Rozinek, J. Mareš, The duality of similarity and metric Spaces, Appl. Sci., 11(4), 1910, (2021).
[10] M. Bukatin, R. Kopperman, S. G. Matthews, H. Pajoohesh, Partial metric spaces, Amer. Math. Monthly, 116(8), 708-718, (2009).
[11] S. G. Matthews, Partial Metric Topology, Ann. New York Acad. Sci., 728, 183-197, (1994).
[12] İ. Altun, F. Sola, H. Şimşek, Generalized contractions on partial metric spaces, Topol. Appl., 157(18), 2778-2785, (2010).
[13] D. Bugajewski, R. Wang, On the topology of partial metric spaces, Math. Slovaca, 70(1), 135-146, (2020).
[14] S. Han, J. Wu, D. Zhang, Properties and principles on partial metric spaces, Topol. Appl., 230, 77-98, (2017).
[15] E. Karapınar, İ. M. Erhan, Fixed point theorems for operators on partial metric spaces, Appl. Math. Lett., 24(11), 1894-1899, (2011).
[16] H.-P. A. Künzi, H. Pajoohesh, M. P. Schellekens, Partial quasi-metrics, Theor. Comput. Sci., 365(3), 237-246, (2006).
[17] S. G. Matthews, An extensional treatment of lazy data flow deadlock, Theor. Comput. Sci., 151(1), 195-205, (1995).
[18] V. Mykhaylyuk, V. Myronyk, Metrizability of partial metric spaces, Topol. Appl., 308, 107949, (2022).
[19] S. Oltra, O. Valero, Banach's Fixed Point Theorem for Partial Metric Spaces, Rend. Istit. Mat. Univ. Trieste, 36, 17-26, (2004).
[20] I. L. Reilly, P. V. Subrahmanyam, M. K. Vamanamurthy, Cauchy Sequences in Quasi-Pseudo-Metric Spaces, Mh. Math., 93, 127-140, (1982).
[21] H.-P. A. Künzi, Nonsymmetric Distances and Their Associated Topologies: About the Origins of Basic Ideas in the Area of Asymmetric Topology, Handbook of the History of General Topology, 853-968, (2001).
[22] H.-P. A. Künzi, V. Vajner, Weighted quasi-metrics, Ann. New York Acad. Sci., 728, 64-77, (1994).
[23] W. A. Wilson, On quasi-metric spaces, Amer. J. Math., 53(3), 675-684, (1931).
[24] M. J. Campión, R. G. Catalán, E. Induráin, O. Valero, Weightable quasi-metrics related to fuzzy sets, Hacettepe Journal of Mathematics and Statistics, 47(5), 1184-1195, (2018).

Bilecik Seyh Edebali University, Department of Mathematics, Faculty of Sciences, Bilecik, Türkiye
Email address: mehmet.solgun@bilecik.edu.tr

Bilecik Seyh Edebali University, Department of Mathematics, Faculty of Sciences, Bilecik, Türkiye
Email address: kemal.taskopru@bilecik.edu.tr

Bilecik Seyh Edebali University, Department of Mathematics, Faculty of Sciences, Bilecik, Türkiye
Email address: 9136510@ogrenci.bilecik.edu.tr

IFSCOM-E 2024
10th Ifs And Contemporary Mathematics and Engineering Conference
04-07 September 2024, Mersin, Türkiye
ISBN:978-625-97923-1-6
pp:109-114

ON SOME ALGEBRAIC CONCEPTS OF SYMBOLIC PLITHOGENIC AND NEUTROSOPHIC RINGS

HAMIYET MERKEPÇI

0000-0003-4302-1162

Abstract. Symbolic logic is a popular subject that has been introduced to theoretical and applied mathematics. The field of study has expanded considerably in recent years. The most famous examples of symbolic structures are neutrosophic structures and symbolic plitogenic structures which have developed using symbolic logic. Neutrosophic numbers and symbolic plitogenic numbers have transferred to algebraic structures such as rings, groups, fields, modules, vector spaces, matrices and their algebraic properties are examined. In this paper, idempotent and nilpotent elements are examined in neutrosophic and symbolic plithogenic rings. The similarities and differences of the algorithms for finding idempotent and nilpotent elements in these two rings are presented. For easy understanding, they are supported with examples.

1. Introduction

Symbolization in mathematical science has become important in recent years. There are many subjects that have brought to the science of mathematics by making use of symbolization. Symbolization has used especially in fields such as theoretical mathematics, topology, data analysis, cryptographic theory and statistics. The most famous examples of the use of symbolization are neutrosophic structures, symbolic plithogenic structures, Turiyam structures. Neutrosophy is a philosophy. It has introduced to mathematics by F. Smarandache in 1980. Neutrosophy has developed fuzzy sets by extending logic and classical probability. It involves uncertainty beyond right and wrong. Therefore, it allows more accurate decisions in various problems of daily life. It has high applicability in decision-making problems [1]. This theory has also been discussed in algebraic structures such as neutrosophic sets, neutrosophic rings, [2-5], neutrosophic vector spaces [6,7], neutrosophic modules [8,9]. Later, F. Smarandache defined n-refined neutrosophic sets and n-cyclic refined neutrosophic sets by dividing the symbol I, which represents uncertainty, into n pieces and defining different products on them. These new sets have been applied to algebraic structures, expanding the field of application and providing

Date: September, 20, 2024.
2000 *Mathematics Subject Classification.* 03A99.
Key words and phrases. Neutrosophic ring, Symbolic plithogenic ring, Idempotent, Nilpotent.

tools that can be used for more complex situations. Refined neutrosophic rings [10-13], n-refined neutrosophic rings [14,15], n-refined neutrosophic modules [16], n-refined neutrosophic spaces and matrices [17,18] are some studies in the literature. Although the elements of the n-refined neutrosophic ring and the n-cyclic refined neutrosophic ring are exactly the same, they have been introduced into mathematics as two different types due to the difference in the multiplication of the uncertainty symbol I. Another example of symbolization is symbolic plithogenic structures. The concept of symbolic plithogenic structures has also presented by Smarandache. Although this structure is similar to n-refined neutrosophic structures, it differs from each other due to the difference in the definition of the product of the symbol used. Symbolic plitogenic numbers have also been defined and studied on algebraic structures such as symbolic plithogenic rings, modules, vector spaces and matrices . Some of the studies on Symbolic Plitogenic structures are as in [19-26]. In this paper, idempotent and nilpotent elements are examined in neutrosophic and symbolic plithogenic rings which have developed using symbolic logic. In order to present the subject within a certain framework and understand its most basic form, idempotent and nilpotent elements in symbolic plithogenic ring such as symbolic 2-plithogenic ring and symbolic 3-plithogenic ring, neutrosophic ring, refined neutrosophic ring have been investigated. The similarities and differences of the algorithms for finding idempotent and nilpotent elements in these two rings, which are similar in structure, are presented. For easy understanding, they are supported with examples.

2. Basic Definitions and Theorems

Definition 2.1. Let R is a ring. The set $2-SP_R = \{a_0 + a_1P_1 + a_2P_2 : a_i \in R, P_i^2 = P_i, P_i.P_j = P_{max(i,j)}\}$ is called symbolic 2-plithogenic ring.

Example 2.2. $R = Z_5 = \{0, 1, 2, 3, 4\}$. $2-SP_{Z_5} = \{a_0+a_1P_1+a_2P_2 : a_i \in Z_5, i = 0, 1, 2\}$

Definition 2.3. Let $2 - SP_R$ be a symbolic 2-plithogenic ring.If an element a in $2 - SP_R$ provides $a^2 = a$, the element is called idempotent.

Theorem 2.4. *Let $A = a_0 + a_1P_1 + a_2P_2$, then A is idempotent if and only if a_0,$a_0 + a_1$,$a_0 + a_1 + a_2$ are idempotent.*

Proof. Let $A = a_0 + a_1P_1 + a_2P_2$. Now compute $A^2 = A$.
$A^2 = A.A = (a_0 + a_1P_1 + a_2P_2)(a_0 + a_1P_1 + a_2P_2)$=$a_0^2 + (a_0a_1 + a_1a_0 + a_1^2)P_1 + (a_0a_2 + a_2a_0 + a_1a_2 + a_2a_1 + a_2^2)P_2$
$\implies a_0^2 = a_0$ (1)
$\implies 2a_0a_1 + a_1^2 = a_1$ (2)
$\implies 2a_0a_2 + 2a_1a_2 + a_2^2 = a_2$ (3)
From equation (1) a_0 is idempotent.
By adding (1) to (2), have $(a_0+a_1)^2 = a_0+a_1$.This means that $a_0+a_1$is idempotent.
By adding (1) to (2) and (3), have $(a_0 + a_1 + a_2)^2 = (a_0 + a_1 + a_2)$.This means that $a_0 + a_1 + a_2$ is idempotent. So, $A^2 = A$ is obtained. □

Example 2.5. Consider $R = Z_6$. $2-SP_R = \{a_0+a_1P_1+a_2P_2 : a_i \in Z_6, i = 0, 1, 2\}$ be symbolic 2-plithogenic ring and $P_1 + 2P_2$, $3P_1 + P_2$, $3 + 4P_1 + 2P_2$, $4P_1 + 3P_2$, $4P_1 + 5P_2$, $P_1 + 5P_2$ are some of symbolic 2-plithogenic idempotent elements.

Definition 2.6. Let $2-SP_R$ be a symbolic 2-plithogenic ring.If an element a in $2-SP_R$ provides $a^n = 0, (n \in Z^+)$, the element is called nilpotent.

Theorem 2.7. *Let A=$a_0+a_1P_1+a_2P_2$, then A is nilpotent if and only if a_0,a_0+a_1, $a_0+a_1+a_2$ are nilpotent.*

Proof. Let A=$a_0+a_1P_1+a_2P_2$, it can be expressed in the form $A^n = a_0^n + [(a_0 + a_1)^n - a_0^n]P_1 + [(a_0 + a_1 + a_2)^n - (a_0 + a_1)^n]P_2$ for all $n \in Z^+$, [*see*19]. So, if $A = a_0 + a_1P_1 + a_2P_2$ is nilpotent, then $A^n = 0$. Hence,
$a_0^n == 0$.
$(a_0 + a_1)^n - a_0^n = 0 \implies (a_0 + a_1)^n = 0$.
$(a_0 + a_1 + a_2)^n - (a_0 + a_1)^n = 0 \implies (a_0 + a_1 + a_2)^n = 0$ □

Example 2.8. Consider $R = Z_8 = \{0, 1, 2, 3, 4, 5, 6, 7\}$. Nilpotent elements in $2-SP_{Z_8}$ are $0, 2, 2P_1, 2P_2, 2+2P_1, 2+2P_2, 2P_1+2P_2, 2+2P_1+2P_2, 4, 4P_1, 4P_2, 4+4P_1, 4+4P_2, 4P_1+4P_2, 4+4P_1+4P_2, 2+6P_1+4P_2$.

Definition 2.9. Let R is a ring. The set $3-SP_R = \{a_0 + a_1P_1 + a_2P_2 + a_3P_3 : a_i \in R, P_i^2 = P_i, P_i.P_j = P_{max(i,j)}\}$ is called symbolic 3-plithogenic ring.

Example 2.10. $R = Z_6 = \{0, 1, 2, 3, 4, 5\}$. $3-SP_{Z_6} = \{a_0 + a_1P_1 + a_2P_2 + a_3P_3 : a_i \in Z_6, i = 0, 1, 2, 3\}$
$X = 2+3P_1+5P_2+P_3$, $Y = 1+P_1+4P_2+3P_3$, then, $X+Y = 3+4P_1+3P_2+4P_3$, $X - Y = 1 + 2P_1 + P_2 + 4P_3$, $X.Y = 2 + 2P_1 + 8P_2 + 6P_3 + 3P_1 + 3P_1 + 12P_2 + 9P_3 + 5P_2 + 5P_2 + 20P_2 + 15P_3 + P_3 + P_3 + 4P_3 + 3P_3 = 2 + 2P_1 + 2P_2 + 3P_3$.

Definition 2.11. Let $3-SP_R$ be a symbolic 3-plithogenic ring.If an element a in $3-SP_R$ provides $a^2 = a$, the element is called idempotent.

Theorem 2.12. *Let $A = a_0 + a_1P_1 + a_2P_2 + a_3P_3$, then A is idempotent if and only if a_0,$a_0 + a_1$,$a_0 + a_1 + a_2$, $a_0 + a_1 + a_2 + a_3$ are idempotent.*

Proof. Let $A = a_0 + a_1P_1 + a_2P_2 + a_3P_3$. Now compute $A^2 = A$.
$A^2 = A.A = (a_0 + a_1P_1 + a_2P_2 + a_3P_3)(a_0 + a_1P_1 + a_2P_2 + a_3P_3)$=$a_0^2 + (a_0a_1 + a_1a_0 + a_1^2)P_1 + (a_0a_2 + a_2a_0 + a_1a_2 + a_2a_1 + a_2^2)P_2 + (a_0a_3 + a_3a_0 + a_1a_3 + a_3a_1 + a_2a_3 + a_3a_2 + a_3^2)P_3$
$\implies a_0^2 = a_0$ (1)
$\implies a_0a_1 + a_1a_0 + a_1^2 = a_1$ (2)
$\implies a_0a_2 + a_2a_0 + a_1a_2 + a_2a_1 + a_2^2 = a_2$ (3)
$\implies a_0a_3 + a_3a_0 + a_1a_3 + a_3a_1 + a_2a_3 + a_3a_2 + a_3^2 = a_3$ (4)
From equation (1) a_0 is idempotent.
By adding (1) to (2), have $(a_0+a_1)^2 = a_0+a_1$.This means that $a_0+a_1$is idempotent. By adding (1) to (2) and (3), have $(a_0 + a_1 + a_2)^2 = (a_0 + a_1 + a_2)$.This means that $a_0 + a_1 + a_2$ is idempotent. By adding (1) to (2) to (3) to (4), have $(a_0 + a_1 + a_2 + a_3)^2 = (a_0 + a_1 + a_2 + a_3)$.This means that $a_0 + a_1 + a_2 + a_3$ is idempotent.So, $A^2 = A$ is obtained. □

Example 2.13. Consider $R = Z_6$. $3-SP_R = \{a_0+a_1P_1+a_2P_2+a_3P_3 : a_i \in Z_6, i = 0, 1, 2, 3\}$ be symbolic 3-plithogenic ring and $1+3P_1+5P_2+3P_3$, $1+5P_1+3P_2+3P_3$, $3 + P_1 + 2P_2 + 3P_3$, $1 + 3P_2 + 2P_3$ are some of symbolic 3-plithogenic idempotent elements.

Definition 2.14. Let $3-SP_R$ be a symbolic 3-plithogenic ring.If an element a in $3-SP_R$ provides $a^n = 0, (n \in Z^+)$, the element is called nilpotent.

Theorem 2.15. *Let A=$a_0 + a_1P_1 + a_2P_2 + a_3P_3$, then A is nilpotent if and only if a_0,$a_0 + a_1$, $a_0 + a_1 + a_2$, $a_0 + a_1 + a_2 + a_3$ are nilpotent.*

Proof. Let A=$a_0 + a_1P_1 + a_2P_2 + a_3P_3$, it can be expressed in the form $A^n = a_0^n + [(a_0+a_1)^n - a_0^n]P_1 + [(a_0+a_1+a_2)^n - (a_0+a_1)^n]P_2 + (a_0+a_1+a_2+a_3)^n - (a_0+a_1+a_2)^n$ for all $n \in Z^+$, [*see*24]. So, if $A = a_0+a_1P_1+a_2P_2+a_3P_3$ is nilpotent, then $A^n = 0$. Hence,
$a_0^n = 0$.
$(a_0 + a_1)^n - a_0^n = 0 \implies (a_0 + a_1)^n = 0$.
$(a_0 + a_1 + a_2)^n - (a_0 + a_1)^n = 0 \implies (a_0 + a_1 + a_2)^n = 0$
$(a_0 + a_1 + a_2 + a_3)^n - (a_0 + a_1 + a_2)^n = 0 \implies (a_0 + a_1 + a_2 + a_3)^n = 0$

□

Example 2.16. Consider $R = Z_8 = \{0, 1, 2, 3, 4, 5, 6, 7\}$. Some of nilpotent elements in $3 - SP_{Z_8}$ are 0, 2, 4, $2 + 2P_1 + 2P_2 + 2P_3$, $4 + 4P_1 + 4P_2 + 4P_3$, $2 + 6P_1 + 4P_2 + 4P_3$.

Definition 2.17. A neutrosophic ring over an any ring R is defined as $R(I) = \{a + bI : a, b \in R\}$ where I is a neutrosophic element with $I^2 = I$.

Example 2.18. Z(I), Q(I), $\mathbb{R}(I)$, $\mathbb{C}(I)$ are neutrosophic rings of integer, rational, real and complex numbers, respectively.

Definition 2.19. Let $R(I)$ be a neutrosphic ring. If an element a in $R(I)$ provides $a^2 = a$, the element is called idempotent element.

Definition 2.20. Let $R(I)$ be a neutrosphic ring.Then $a = m+nI \in R(I)$ is called a neutrosophic idempotent element if $n \neq 0$ and $a^2 = a$.

Example 2.21. Let $R = Z_2$. Idempotent elements of Z_2 are 0,1 and neutrosophic idempotent element is I.

Example 2.22. In the neutrosophic ring $Z_3(I)$, I and $1 + 2I$ are neutrosophic idempotent elements.

Definition 2.23. $R(I)$ be a neutrosophic ring.For all $x, y \in R(I)$, if $xy = yx$ then $R(I)$ is a commutative neutrosophic ring. In addition, there exists $1 \in R(I)$ such that $\forall x \in R(I)$, $1.x = x.1 = x$ thus $R(I)$ is a commutative neutrosophic ring with unity.

Definition 2.24. [13] R is a ring and $R(I)$ is a commutative neutrosophic ring. Let $a = m + nI \in R(I)$ with $m, n \in R$.
1. For an integer $k > 0$ and $m, n \neq 0$ if $a^k = 0$, then a is called a strong neutrosophic nilpotent element.
2. For an integer $k > 0$ and $m = 0$, $n \neq 0$ if $a^k = 0$, then a is called a weak neutrosophic nilpotent element.
3. For an integer $k > 0$ and $n = 0$, if $a^k = 0$, then a is called an ordinary nilpotent element.

Example 2.25. $Z_4(I)$ is the neutrosophic ring of integer modulo 4, 0 and 2 are ordinary nilpotent elements, $2I$ is a weak nilpotent element and $2 + 2I$ is a strong neutrosophic element.

Definition 2.26. [17] R be a ring and I split into $I_1, I_2, ..., I_n$. Then $R_n(I) = \{x_0 + x_1I_1 + x_2I_2 + ... + x_nI_n : x_i \in R\}$ is called n-refined neutrosophic ring with multiplication of $I_1, I_2, ..., I_n$ is $I_i.I_j = I_{min(i,j)}$.

Definition 2.27. Let $X = A_0 + A_1I_1 + A_2I_2 + ...A_nI_n$ be an n-refined neutrosophic element; ıts canonical sequences are defined as follows:
$M_0 = A_0$, $M_j = A_0 + A_j + A_{j+1} + ... + A_n; 1 \leq j \leq n$. For instance; $M_4 = A_0 + A_4 + A_5 + ... + A_n$.

Theorem 2.28. *Let $X = A_0 + A_1I_1 + ... + A_nI_n$ be an n-refined neutrosophic element, then*
(a) X is nilpotent if and only if M_j are nilpotent, for all j.
(b) X is idempotent if and only if M_j are idempotent, for all j.

Proof. It can be seen in [17]. □

3. Conclusion

Neutrosophic numbers and symbolic plithogenic numbers are a concept that have been researched in the field of mathematics for a long time and used in different algebraic structures. A new improvement has been brought to number theory, especially by carrying out studies on neutrosophic numbers and symbolic plithogenic numbers on rings. An important topic of these studies is idempotent and nilpotent elements in rings. The concept of neutrosophic rings is further sub divided into categories such as refined neutrosophic rings, n-refined neutrosophic rings and the concept of symbolic plithogenic ring such as symbolic 2-plithogenic ring and symbolic 3-plithogenic ring.In this paper, idempotent and nilpotent elements found in different types of neutrosophic rings and symbolic plithogenic ring are examined. In particular, a study on the determination of idempotent and nilpotent elements in neutrosophic ring, n-refined neutrosophic ring,symbolic 2-plithogenic ring and symbolic 3-plithogenic ring, is presented. For easy understanding, they are supported with examples. They are still a nascent field and there are many open problems to be discovered in this field. Therefore, this study may inspire future research.

References

[1] M.Abdel-Basset, A.Gamal,, R. K.Chakrabortty and M.Ryan, A new hybrid multi-criteria decision-making approach for location selection of sustainable offshore wind energy stations: A case study, Journal of Cleaner Production, 280, 124462,(2020).
[2] V.W.B.Kandasamy, F.Smarandache, Some Neutrosophic Algebraic Structures and Neutrosophic N-Algebraic Structures, Hexis, Phonex, Arizona, (2006).
[3] V.W.B.Kandasamy, F.Smarandache , Neutrosophic Rings, Hexis, Phoenix,Arizona, (2006).
[4] M.Abobala, On Some Special Substructures of Neutrosophic Rings and Their Properties, International Journal of Neutrosophic Science, 4, 72-81, (2020).
[5] Y.Ceven and S.Tekin, Some Properties of Neutrosophic Integers, Kırklareli University Journal of Engineering and Science, 6, 50-59, (2020).
[6] M.Abobala, AH-Subspaces in Neutrosophic Vector Spaces, International Journal of Neutrosophic Science, 6, 80-86,(2020).
[7] V.W.B.Kandasamy, F.Smarandache, Some Neutrosophic Algebraic Structures and Neutrosophic N-Algebraic Structures, Hexis, Phonex, Arizona,(2006).
[8] M.Abobala, R.Alhamido, AH-Substructures in Neutrosophic Modules, International Journal of Neutrosophic Science, 7, 79-86,(2020).
[9] W.B. V. Kandasamy, F.Smarandache , Neutrosophic Rings, Hexis, Phoenix,Arizona, (2006).
[10] M.Abobala, On Refined Neutrosophic Matrices and Their Applications In Refined Neutrosophic Algebraic Equations, Journal Of Mathematics, Hindawi,(2021).
[11] E.O.Adeleke, A.A.A.Agboola, F.Smarandache, Refined Neutrosophic Rings II, International Journal of Neutrosophic Science, Vol. 2(2), 89-94, (2020).
[12] A.A.A.Agboola , A.D.Akinola, O.Y.Oyebola , Neutrosophic Rings I, International J.Math. Combin, 4, 1-14, (2011).

[13] A.A.A.Agboola, E.O.Adeleke, S.A.Akinleye , Neutrosophic Rings II, International J.Math. Combin, 2, 1-8, (2012).
[14] M.Abobala, A Study of Maximal and Minimal Ideals of n-Refined Neutrosophic Rings, Journal of Fuzzy Extension and Applications, 2, 16-22,(2021).
[15] H,Sankari, M.Abobala, Neutrosophic Linear Diophantine Equations With Two Variables, Neutrosophic Sets and Systems, 38, 399-408, (2020).
[16] H.Sankari, M.Abobala, n-Refined Neutrosophic Modules, Neutrosophic Sets and Systems, 36, 1-11,(2020).
[17] M.Abobala, On Some Algebraic Properties of n-Refined Neutrosophic Elements and n-Refined Neutrosophic Linear Equations, Mathematical Problems in Engineering, Hindawi, (2021).
[18] F.Smarandache, M.Abobala, n-Refined Neutrosophic Vector Spaces, International Journal of Neutrosophic Science, 7, 47-54, (2020).
[19] H.Merkepci, M.Abobala, On The Symbolic 2-Plithogenic Rings, International Journal of Neutrosophic Science, 20(3), 115-122, (2023).
[20] N.Taffach, An Introduction to Symbolic 2-Plithogenic Vector Spaces Generated from The Fusion of Symbolic Plithogenic Sets and Vector Spaces, Neutrosophic Sets and Systems, 54, (2023).
[21] N.Taffach, K.Ben Othman, An Introduction to Symbolic 2-Plithogenic Modules Over Symbolic 2-Plithogenic Rings, Neutrosophic Sets and Systems, 54, (2023).
[22] F.Smarandache, Introduction to the Symbolic Plithogenic Algebraic Structures (revisited), Neutrosophic Sets and Systems, 53, (2023).
[23] F.Smarandache, Plithogenic Algebraic Structures, Chapter in "Nidus idearum Scilogs, V: joining the dots" (third version), Pons Publishing Brussels, 123-125, (2019).
[24] O.Albasheer, A.Hajjari, R.Dalla, On The Symbolic 3-Plithogenic Rings and Their Algebraic Properties, Neutrosophic Sets and Systems, 54, (2023).
[25] H.Merkepci, A.Rawashdeh, On The Symbolic 2-Plithogenic Number Theory and Integers , Neutrosophic Sets and Systems, 54, (2023).
[26] A.Khaldi, K.Ben Othman, O.Von Shtawzen, R.Ali, S.Mosa, On Some Algorithms for Solving Different Types of Symbolic 2-Plithogenic Algebraic Equations, Neutrosophic Sets and Systems, 54, (2023).

Department of Mathematics, Faculty of Art and Science, Gaziantep, Türkiye
Email address: hamiyetmerkepci@hotmail.com

4 SEPTEMBER 2024

REGISTRATION
13:00-14:00

OPENNING CEREMONY
Assoc. Prof. Dr. Gökhan Çuvalcıoğlu
14:00-14:45

KEYNOTE SPEAKER
The Process of Predictions and Programming
Prof. Dr. Kenan Peker
Chair: Gökhan Çuvalcıoğlu
15:00-15:45

COFFEE BREAK
15:45-16:00

	HALL-A		HALL-B
	Chair:		Chair:
16:00-16:15	A Computational Algorithm For Solutions Of System Of Fractional Order Differential Equations **Elçin Gökmen**	16:00-16:15	Limited Operators On Banach Lattices **Nefise Nur Begüm Kayacı**, Ömer Gök
16:15-16:30	Method Of The Exact Difference Schemes For The Integro-Differential Equations With Boundary Layers **Muhammet Enes Durmaz**	16:15-16:30	On The Extension Of Conformable Fractional Dynamic Dirac System **Yasin Ertuğrul,** Hüseyin Tuna
16:30-16:45	The Main Equation Of Inverse Scattering Problem Of Sturm-Liouville Operator Containing Spectral Parameter **Özge Akçay**	16:30-16:45	On The Reducibility Of Weighted Composition Operators Teube Cyrille Mbainaissem, **Dethie Dione**
16:45-17:00	Solving Sturm-Liouville Problems Using Mathematica Software **Fikret Doğan Bakoğlu**, Kh.R. Mamedov	16:45-17:00	Similarity Metric And Its Relations Between Other Metrics Mehmet Solgun, Kemal Taşköprü, **Esra Güder**
17:00-17:15	Comprehensive Analysis Of Fuzzy C-Means Clustering And Its Variants **Orkun Gürler,** Efendi Nasibov	17:00-17:15	On The Problem Of Computing Projectivities Between Rational Vector Fields **Uğur Gözütok**

KEYNOTE SPEAKER

Optimization of Type-2 Fuzzy Systems and Future Trends for Theory and Applications

Prof. Dr. Oscar Castillo

Chair: Gökhan Çuvalcıoğlu

17:30-18:15

5 SEPTEMBER 2024

	HALL-A		HALL-B
	Chair:		Chair:
09:00-09:15	Dynamics Properties Of A Discrete Time Model With Weak Allee Effect **Figen Kangalgil,** Seval Işık	09:00-09:15	Comparative Study Of Solar PV Storage For Utility Scales Applications Danladi Garba, **Collins N. Ineneji**
09:15-09:30	Another Example For *P*-Ideals **Mustafa Gülfırat**	09:15-09:30	Design And Electromagnetic Analysis Of Magnetically Controlled Shunt Reactor **İres İskender,** Emir Yükselen
09:30-09:45	On Alternating Bicommutative Polynomials **Nazar Şahin Öğüşlü**	09:30-09:45	Modeling Neuron Growth Using Artificial Neural Networks **Brishna Khan**
09:45-10:00	Convergence Of Bieberbach Polynomials In Special Domains **Cem Koşar**	09:45-10:00	Evaluating The Effects Of Refrigerant Charge Levels On ASHP Operating Parameters **Kutbay Sezen**

COFFEE BREAK

10:00-10:15

INVITED SPEAKER

Intuitionistic Fuzzy l-Ideals and Intuitionistic Fuzzy l-Filters in l-Groups

Prof. Dr. P.K. Sharma

Chair: Gökhan Çuvalcıoğlu

10:15-11:00

COFFEE BREAK

11:00-11:15

	HALL-A		HALL-B

	Chair:		Chair:
11:15-11:30	On Some Algebraic Concepts Of Symbolic Plithogenic And Neutrosophic Rings **Hamiyet Merkepçi**	11:15-11:30	Multiple-Layer Microstrip Circular Patch Antenna Array As A Solution For Significant Improvement In Gain, Directivity, And Multiple Band Frequency Antenna Danladi Garba, **Collins N. Ineneji**
11:30-11:45	Korovkin Type Convergence Theorems And Their Applications **Cem Koşar**, Nida Palamut Koşar	11:30-11:45	Investigation Of Mechanical Properties Of Fly Ash-Based 3D-Printed Geopolymer Mortars **Maksut Seloğlu**
11:45-12:00	On $\mathbb{Z}_4$-Invariants Of Algebras Of Generic Objects **Nazar Şahin Öğüşlü**	11:45-12:00	Numerical Analysis Of A Phase Change Material-Based Thermal Control System For Small Satellites **Burak İzgi**
12:00-12:15	On Hybrid Matrix Pencils **Emel Karaca**	12:00-12:15	The Effect Of The Use Of Paraffin Wax On The Regression Rate Of Hybrid Rocket Engines: A Review **Süreyya Sevinç Varol**, Bilge Albayrak Çeper, Nafiz Kahraman
12:15-12:30	Some Applications In Education Using Intuitionistic Fuzzy Sets **Ali Sınar**, Erhan Çetinkaya and Celalettin Akdoğan	12:15-12:30	

LUNCH
12:30-13:00

INVITED SPEAKER
Invariant Theory of Concrete Finite Groups
Prof. Dr. Şehmus Fındık
Chair: Gökhan Çuvalcıoğlu
13:00-13:45

COFFEE BREAK
13:45-14:00

	HALL-A		HALL-B
	Chair:		Chair:
14:00-14:15	On The Application Of The Fractional Order Obesity Model **Zafer Öztürk**	14:00-14:15	An Evaluation And Ranking Approach For E-Commerce Websites Based On Spherical Fuzzy Sets Under Industry 4.0 **Erdem Aksakal,** Zeynep Durmaz
14:15-14:30	Some Identities For Sequences Of Binomial Sums Of Generalized Padovan Identities Including Powers And Binomial Coefficients **Orhan Dişkaya**	14:15-14:30	The Effect Of Question Order On Exam Performance: An Example For Civil Engineering Students **Feride Maide Mızrakçı,** Savaş Bayram
14:30-14:45	On A Generalization Of The Hosoya Triangle **Turhan Çifçi**, Hamza Menken, Orhan Dişkaya	14:30-14:45	Human Factors-Based Design And Structural Analysis Of Military-Grade Ladder

			İlayda Aldatmaz, Mustafa Tellioğlu, Selin Selen Eroğlu
14:45-15:00	On Oscillation Of Linear Dynamic Equations Under Impulse Effects **Sibel Doğru Akgöl**, Ağacık Zafer	14:45-15:00	
COFFEE BREAK 15:00-15:15			
	HALL-A		HALL-B
	Chair:		Chair:
15:15-15:30	Geometry Of Screen Generic Transversal Lightlike Submanifolds Of Indefinite Kaehler Manifolds **Nergiz Önen Poyraz**, Mehmet Akif Akyol	15:15-15:30	Frequency Constraint Handling Truss Optimization Using Bonobo Optimizer **İbrahim Behram Uğur**
15:30-15:45	A Dynamic Approach To The Fractional Order Prey-Predator Population Model **Zafer Öztürk**	15:30-15:45	Structural Optimization Of Military Type Electronic Cabinet **İlayda Aldatmaz,** Kaan Kartal, Anıl Açar
15:45-16:00	On A Class Of Fractional Impulsive Dynamic Equations On Time Scales **Sibel Doğru Akgöl**, Svetlin G. Georgiev	15:45-16:00	Flux Pinning Properties of Nano-Size Zn Doped Bi-2212 Superconductors **Mehmet Ersin Aytekin**
16:00-16:15	Multi-Step Trigonometric Cubic B-Spline Least –Squares Method For Regularized Long Wave Equation Bülent Saka, **Ömer Yazar**	16:00-16:15	
COFFEE BREAK 16:15-16:30			
	HALL-A		HALL-B
	Chair:		Chair:
16:30-16:45	Integration Of The Type 2 Neutrosophic Fuzzy Sets And Scope Validity Ratio (Lawshe) Approach To Identify The Influential Criteria To Structure Of The Decision-Making Problems **Ömer Faruk Görçün**, Hande Küçükönder	16:30-16:45	Random Vibration Analysis And Evaluation Of The Military Vehicle Afes In Open And Closed Positions Under MIL-STD-810g **Selin Selen Eroğlu,** İlayda Aldatmaz, Furkan Güleryüz
16:45-17:00	Stock Selection Using Multi Criteria Decision Making Methods on Intuitionistic Fuzzy Set Based Mehmet Çitil, **Mehmet Emin Akkurt**	16:45-17:00	Comparative Pyrolysis Kinetics Of Orange And Tangerine Peel **Meltem Kızılca Çoruh**
17:00-17:15	A New Plug And Play Algorithm And Its Applications To Super-Resolution Problem **Eda Nur Yıldırım**, İbrahim Karahan	17:00-17:15	Investigation And Comparing To Other Steel Of Springback Condition In Armor Steels **Mesut Yılmaz**
17:15-17:30	Re-Vısıt $\mathcal{J}*-$Sequentıal Topology **Hassina Sabor Behmanush**, Mehmet Küçükaslan		
GALA DINNER 19:00			

6 SEPTEMBER 2024

INVITED SPEAKER

The Energy of a Graph Over Real Neutrosophic Fuzzy Weights

Prof. Dr. Madhumangal Pal

Chair: Gökhan Çuvalcıoğlu

09:00-09:45

COFFEE BREAK

09:45-10:00

	HALL-A		HALL-B
	Chair:		Chair:
10:00-10:15	New Optical Soliton Solutions To The (3+1)-Dimensional Nonlinear Schrödinger Equation **Sibel Şehriban Ataş**	10:00-10:15	Oscillatory Flow Of Grains Down A Chute With Possible İmpact Phenomena **Samire Yazar**
10:15-10:30	A New Finite Difference Method For The 2D Heat Equation **Özgül İlhan,** Elif Tembelo	10:15-10:30	Comparison Of Methods Used in Predicting National Electricity Energy Consumption Amounts And An Application With United Kingdom Data **Nefise Ertoy,** Mehmet Akansel
10:30-10:45	The Congruity Of Solutions From Stochastic And Random Models In The Analysis Of Deterministic Systems With Uncertainty **Zafer Bekiryazıcı**	10:30-10:45	The Potential Of Ginsenosides As An Alternative To Anthracyclines In Breast Cancer Treatment: An In Silico Study Nil Sazlı, **Deniz Karataş**
10:45-11:00	Algebraic Properties of Controlled Sets Gökhan Çuvalcıoğlu, **Dilara Gündoğdu**	10:45-11:00	Gps Data Synchronisation Using Kalman Filter **Yusuf İslam Budak**, Ali Köse, Pegah Mutlu

COFFEE BREAK

11:00-11:15

	HALL-A		HALL-B
	Chair:		Chair:
11:15-11:30	Some Novel Characteristics Of A New Variant Of Bernstein Operators **Nezihe Turhan Turan**	11:15-11:30	Examination Of Reasons For Leaving A Job With The Mcdm Method **Özgür Zateri,** Serap Akcan Yetgin
11:30-11:45	A New Finite Difference Method For The First Order Wave Equation **Özgül İlhan,** Günay Ergun Bülbül	11:30-11:45	Evolving Flow Of A Grain In A Branching Channel **Samire Yazar**
11:45-12:00	A Non Commutative Determinant Of Invertible Matrices On Universal Enveloping Algebras Of Free Leibniz Algebras **Zeynep Özkurt**	11:45-12:00	Vibration Analysis Of Functionally Graded Microbeams Based On Modified Couple Stress Theory **Duygu Atcı**

12:00-12:15	Intuitionistic Fuzzy Entropies And Their Roles In Decision Making Processes Gökhan Çuvalcıoğlu, **Feride Tuğrul**, Arif Bal	12:00-12:15	A Pi Algorithm Based Approach For Optimum Parameter Estimation Of Rayleigh Distribution In Wind Energy Applications **Hilmi Aygün,** Bayram Köse
12:15-12:30		12:15-12:30	A Lexiographic Goal Programming Approach For Solving Multiple Goals In An E-Commerce Distribution Warehouse System **Ela Binici Fayetörbay**, Erdem Aksakal
LUNCH 12:30-13:30			
	HALL-A		HALL-B
	Chair:		Chair:
13:30-13:45	On Elliptic Sombor Index Of Zero Divisor Graphs **Fatma Tirik**, Yaşar Nacaroğlu	13:30-13:45	On Invariants Of The Metabelian Product **Nazar Şahin Öğüşlü**
13:45-14:00	Applications Of Non-Commutative Determinants: Non-Tame Automorphisms **Zeynep Özkurt**	13:45-14:00	A Minimal Maslov Number Condition For Displaceability In Certain Weakly Exact Symplectic Manifolds **Nil İpek Şirikçi**
14:00-14:15	Hyper-Dual Numbers Related To Generalized Tribonacci Numbers **Tülay Yağmur**	14:00-14:15	Existence Results For A P-Laplacian Caputo-Type Fractional Boundary Value Problem Via Fixed Point Theory **Tuğba Şenlik Çerdik**, Fulya Yörük Deren
14:15-14:30	The Effect Of Hesitation Degree On Decision Making Processes And Criteria Weights **Feride Tuğrul**	14:15-14:30	Some Results On *I*-Deferred Statistical Convergence Of Order Alpha Sequences In Paranormed Spaces **Zeynep Hande Toyganözü**
COFFEE BREAK 14:30-14:45			
	HALL-A		HALL-B
	Chair:		Chair:
14:45-15:00	Theoretical Improvements on Decomposed Fuzzy Sets **Ali Köseoğlu**	14:45-15:00	Subcategories Of Modules And Irreducible Representations Of Leavitt Path Algebras With Coefficients in A Commutative Ring **Ayten Koç**
15:00-15:15	$[\alpha, \beta]$- Bounded Intuitionistic Fuzzy Sets And Subgroups **Ümit Deniz**	15:00-15:15	On Solutions Of Some Generalized Functional Equations Arising İn Mathematical Psychology And Theory Of Learning **Ali Turab**
15:15-15:30	Gradation Of Intuitionistic Fuzzy Functions Ümit Deniz, **Neslihan Yilmaz**	15:15-15:30	
15:30-15:45	Comparison Of Two Iterative Algorithms For Root Finding **Şükran Konca**, Bayram Köse, Bahar Demirtürk	15:30-15:45	

COFFEE BREAK
15:45-16:00

	HALL-A		HALL-B
	Chair:		Chair:
16:00-16:15	Multi-Scale Mathematical Analysis And Modeling Of Glycogenesis Pathways In The Liver **Deniz Öztürk**	16:00-16:15	Leavitt Path Algebras With Coefficients in A Commutative Unital Ring **Ayten Koç**
16:15-16:30	Sequence Spaces And Matrix Domain Of Quintet Band Matrix **Mustafa Cemil Bişgin**	16:15-16:30	The New Study For Solving The Nonlinear Fractional Partial Differantial Equations **Hakkı Güngör**
16:30-16:45	A Study The Conduct Of Differential Identities On Semiprime σ-Rings **Mehsin Jabel Atteya**	16:30-16:45	Radii Problems For Starlike And Convex Functions Associated With Sine And Cosine Functions For Some Basic Arithmetic Operations **Manivannan M**
16:45-17:00	Graph-Theoretical Approaches to Routing Problems in Computer Networks With Path-Coding Methods: Bloom Filter Vs Cuckoo Filter **Gökçe Çaylak Kayaturan**	16:45-17:00	An Integrated AHP-COBRA Approach on Decomposed Fuzzy Sets **Elif Başkan**, Ali Köseoğlu, Rıdvan Şahin
17:00-17:15	Comparison Of Similarity Measures Of Some L-Fuzzy Sets Gökhan Çuvalcıoğlu, **Cansu Altıncı**	17:00-17:15	A Multi-Criteria Decision Making Approach Using a New Similarity Measure Under the Neutrosophic Z-Number Universe **Güler Tuğba Gültekin**, Elif Başkan, Rıdvan Şahin

CLOSING CEREMONY
17:15